An Overview of Antarctic Sea Ice in the Community Earth System Model version 2, Part I: Analysis of the Seasonal Cycle in the Context of Sea Ice Thermodynamics and Coupled Atmosphere-Ocean-Ice Processes

Hansi K.A. Singh[1], Laura Landrum[2], Marika M. Holland[2], David A. Bailey[2], and Alice K. DuVivier[2]

[1]School of Earth and Ocean Sciences, University of Victoria, Victoria BC Canada

[2]Climate and Global Dynamics Laboratory, National Center for Atmospheric Research, Boulder CO USA

Key Points:

- Antarctic sea ice is thinner and less extensive in CESM2 than in CESM1.
- A new mushy-layer thermodynamics formulation in CICE5 accelerates ice growth in coastal polynyas and augments snow-to-ice conversion.
- Greater surface wind stress curl increases warm water upwelling under the ice pack in CESM2, which thins ice and decreases its extent.

Corresponding author: H.K.A. Singh, `hansingh@uvic.ca`

This article has been accepted for publication and undergone full peer review but has not been through the copyediting, typesetting, pagination and proofreading process which may lead to differences between this version and the Version of Record. Please cite this article as doi: 10.1029/2020MS002143

Abstract

We assess Antarctic sea ice climatology and variability in version 2 of the Community Earth System Model (CESM2), and compare it to that in the older CESM1 and (where appropriate) real-world observations. In CESM2, Antarctic sea ice is thinner and less extensive than in CESM1, though sea ice area is still approximately 1 million km^2 greater in CESM2 than in present-day observations. Though there is less Antarctic sea ice in CESM2, the annual cycle of ice growth and melt is more vigorous in CESM2 than in CESM1. A new mushy-layer thermodynamics formulation implemented in the latest version of the Community Ice Code (CICE) in CESM2 accounts for both greater frazil ice formation in coastal polynyas and more snow-to-ice conversion near the edge of the ice pack in the new model. Greater winter ice divergence in CESM2 (relative to CESM1) is due to stronger stationary wave activity and greater wind stress curl over the ice pack. Greater wind stress curl, in turn, drives more warm water upwelling under the ice pack, thinning it and decreasing its extent. Overall, differences between Antarctic sea ice in CESM2 and CESM1 arise due to both differences in their sea ice thermodynamics formulations, and differences in their coupled atmosphere-ocean states.

Plain Language Summary

Sea ice is a central part of the Antarctic climate system, and Earth system models are an indispensable tool for studying the climate of the Antarctic. Advances in modelling are essential for understanding and projecting future changes in the region as the globe warms. Here, we describe Antarctic sea ice climatology in the state-of-the-art Community Earth System Model, version 2 (CESM2). CESM2 incorporates several modelling advances which collectively improve representation of Antarctic climate compared to previous model versions. Among these is a 'mushy layer' treatment of sea ice, where the ice is modelled as a mixture of solid ice and salty water. Modeling sea ice as a mushy layer changes the way that Antarctic sea ice grows in CESM2, in a manner more closely resembling how Antarctic sea ice has been observed to grow in the real world. Antarctic sea ice area in CESM2 also more closely matches observed sea ice area, due primarily to differences in atmospheric winds and ocean heating. In conjunction with observations and other state-of-the-art global climate models, CESM2 will be an important tool for furthering understanding of Antarctic climate at present and in the future.

1 Introduction

Sea ice is a fundamental, dynamic component of the Antarctic climate system. Antarctic sea ice undergoes extraordinary expansion and retreat over the seasons: ice area expands from a mere 2 million km^2 at its end-of-summer minimum to nearly 15 million km^2 at its spring maximum (Gordon, 1981; Parkinson & Cavalieri, 2012). This massive seasonal growth and retreat of ice area impacts nearly every aspect of the Antarctic system, from atmospheric stability and ocean dynamics, to ice sheet mass balance and biological productivity.

The presence of sea ice strongly attenuates (turbulent and radiative) heat and momentum conveyance between the atmosphere and ocean (Eicken, 2003), and the state of the lower troposphere in the high latitudes, including cloudiness, boundary layer depth, and stability, varies substantially with sea ice cover (see, e.g., Wall et al., 2017; Morrison et al., 2018). Sea ice melt and growth impact ocean hydrography through freshwater capping and brine rejection, respectively (Pellichero et al., 2017); brine rejection plays a crucial role in creating low-buoyancy shelf waters off the Antarctic coast that form Antarctic Bottom Water, the coldest and densest water in the world oceans (Goosse et al., 1997; Ohshima et al., 2013). Calving from marine ice shelves, which flow from the Antarctic ice sheet, may be thwarted by the presence of sea ice cover or hastened by its absence (Massom et al., 2018). The Southern Ocean food web, essential for global food security, depends on the seasonal cycle of sea ice, with several keystone species relying on sea ice cover over the course of their developmental cycles (Garrison & Buck, 1989). The Antarctic climate system, both present and future, cannot be understood in full without a reasonable reckoning of the sea ice and its seasonality.

Antarctic sea ice differs in many respects from Arctic sea ice. The magnitude of the seasonal cycle over the Arctic is smaller than that over the Antarctic, with multi-year ice dominating much of Arctic icepack volume historically. Antarctic sea ice is thinner and more extensive (particularly in winter), while Arctic sea ice is thicker and more contained in area (Rothrock et al., 1999; Worby et al., 2008), as the Arctic basin is nearly landlocked by the North American and Eurasian continents. As Antarctic sea ice extends farther equatorward than Arctic sea ice, it is more exposed to fluctuations in the surface westerly wind maximum, and its variability is closely tied to the Southern Annular Mode (SAM; Kwok & Comiso, 2002; Simpkins et al., 2012; Raphael & Hobbs, 2014;

Holland et al., 2017) and related Amundsen Sea Low (Holland et al., 2018). Mechanisms of ice growth and melt also differ between the two hemispheres. Much Antarctic sea ice growth occurs in polynyas off the coast, as downslope (katabatic) winds flow from the high-elevation ice sheet to open coastal waters, driving frazil ice formation (Maqueda et al., 2004; Tamura et al., 2008). Snow falling over the ice pack also thickens Antarctic ice more so than Arctic ice, as snow weight lowers the freeboard below the sea surface, initiating snow-to-ice conversion (Eicken et al., 1995; Massom et al., 2001; Maksym & Markus, 2008). In spring and summer, Antarctic sea ice melts from its base as it retreats to its end-of-summer minimum, while Arctic ice melts at both top and bottom faces nearly equally (Perovich et al., 2014). Such differences between the hemispheres indicate that Antarctic sea ice must be understood as a component in a unique coupled system, distinct from that of the Arctic.

Antarctic sea ice has also responded very differently to a warming climate than Arctic sea ice. While Arctic sea ice has retreated significantly in response to anthropogenic greenhouse gas forcing, Antarctic sea ice underwent a modest expansion from 1979 to 2015. This paradoxical expansion of Antarctic sea ice area, occurring concurrently with increasing global mean surface temperatures and rapid retreat of Arctic sea ice, was initially attributed to stratospheric ozone loss over the Antarctic (J. Turner et al., 2009), or to an increase in freshwater fluxes into the Southern Ocean (due to ice shelf melt, for example; see Bintanja et al., 2013). Later studies suggested that neither the Antarctic ozone hole and associated positive SAM trend (Sigmond & Fyfe, 2010; Bitz & Polvani, 2012; Landrum et al., 2017) nor observed changes in freshwater forcing (Swart & Fyfe, 2013; Pauling et al., 2016) were sufficient to explain Antarctic ice area expansion. Natural variability in sea ice area, either driven by variability in Southern Ocean temperatures (Singh et al., 2019), variability in Southern Ocean deep convection (Zhang et al., 2019), or variability in the tropics (Meehl et al., 2016), appears to be the simplest explanation for Antarctic sea ice area expansion over the satellite era. While Arctic sea ice area has experienced fluctuations due to natural variability over the satellite era (Swart et al., 2015), natural variability may play a greater role in Antarctic sea ice evolution because the response to greenhouse gas forcing, both transient and equilibrium, is weaker in the Antarctic than the Arctic (Armour et al., 2016; Singh et al., 2018).

Changes in Antarctic sea ice impact not only the climate local to the Antarctic, but also climate elsewhere. Idealized atmospheric dynamical core experiments suggest that lower tropospheric heating in the high latitudes, similar to that resulting from sea ice loss, tends to push the eddy-driven jet and storm-track equatorward (McGraw & Barnes, 2016). Experiments which isolate the global climate response to (projected) late 21st century Arctic sea ice loss indicate a range of far-reaching impacts, including equatorward jet shifts in both hemispheres, a northward shift in the Intertropical Convergence Zone, and greater extratropical precipitation in both hemispheres (in a fully-coupled model; see Deser et al., 2015; Blackport & Kushner, 2017; Smith et al., 2017). Similar experiments performed to isolate the global climate response to Antarctic sea ice loss suggest a similar slew of remote responses, albeit weaker than the response to Arctic sea ice loss (England et al., 2018).

Though the local and global climate impacts of Antarctic sea ice are substantial, the study of Antarctic sea ice is hampered by the difficulty of obtaining *in situ* observations from remote regions with extreme climatic conditions. As such, global climate models employing sophisticated sea ice components, in which ice evolution is treated both thermodynamically and dynamically, are indispensable tools for study of the Antarctic climate system and its future fate.

Here, we present the first of a two-part overview of Antarctic sea ice in a newly-developed, state-of-the-art global climate model, version 2 of the Community Earth System Model (CESM2; Danabasoglu et al., 2019). In this study, we focus on seasonal Antarctic sea ice climatology in the CESM2, including the many processes that control ice growth, melt, thickness, and area. In an ensuing companion study, we consider sea ice persistence and predictability, particularly the extent to which the Southern Ocean impacts sea ice predictability in the Antarctic.

The sea ice model in CESM2 is CICE5 (Hunke et al., 2015; Bailey et al., 2020, submitted), which employs a mushy-layer thermodynamics scheme (Feltham et al., 2006; A. Turner & Hunke, 2015), supplanting the constant salinity scheme used in earlier versions of the model (Bitz & Lipscomb, 1999, hereafter BL99). Incorporating prognostic salinity has been shown to improve representation of sea ice growth, melt, the ice thickness distribution, and ocean-ice interactions in both hemispheres in models (Vancoppenolle et al., 2009; A. Turner & Hunke, 2015), making it a significant advance in sea ice modelling.

In our analysis, we compare and contrast Antarctic sea ice pre-industrial climatology in CESM2 to that in the older CESM1 (and, briefly, present-day observations). We first assess differences in sea ice area, extent, and thickness between CESM2 and CESM1. We then consider differences in sea ice growth (§3.1) and melt (§3.2) over the course of the seasonal cycle, and the processes by which ice growth and melt occur in CESM2 compared to CESM1. We then proceed to attribute these differences in the sea ice seasonal cycle to, in some respects, differences in their thermodynamics treatments, or, in other respects, to differences in their coupled atmosphere and ocean counterparts (§3.3). We conclude by discussing several promising future research directions in the coupled evolution of Antarctic sea ice highlighted by our analysis (§4).

2 Methodology

The state-of-the-art version 2 of the Community Earth System Model (CESM2) is described in detail in Danabasoglu et al. (2019). All model components have been updated extensively, incorporating cutting-edge physics essential to accurate simulation of the Earth system. The atmosphere component of CESM2, CAM6 (Bogenschutz et al., 2018), incorporates several parameterization advances, including a new unified atmospheric convection scheme (CLUBB; see Guo et al., 2015; Larson, 2017), updated cloud microphysics (Gettelman & Morrison, 2015; Gettelman et al., 2015), aerosol impacts on cloud formation (i.e. the aerosol indirect effect; see Hoose et al., 2010; Wang et al., 2014; Shi et al., 2015), and more sophisticated treatments of orographic drag (Scinocca & McFarlane, 2000; Beljaars et al., 2004). Other model components, including the land, ocean, and coupler, have also been updated (Danabasoglu et al., 2019).

The new CICE5 is described in depth by Hunke et al. (2015) and Bailey et al. (2020, submitted). The most significant advance in the new model is in the treatment of sea ice as a mushy layer, an amalgam of solid ice interspersed with microscopic pockets of brine (Feltham et al., 2006; A. Turner & Hunke, 2015). In this case, the enthalpy of the ice, q, is a weighted average of the enthalpy of the ice, q_i, and the enthalpy of the brine, q_{br}:

$$q = (1 - \phi)q_i + \phi q_{br} \ , \tag{1}$$

where ϕ is the fraction of the sea ice mush made up of liquid brine. The enthalpy of the ice evolves according to

$$\frac{\partial q}{\partial t} = \frac{\partial}{\partial z}\left(K\frac{\partial T}{\partial z}\right) + w\frac{\partial q_{br}}{\partial z} + F \ , \tag{2}$$

where T is the temperature of the mush, K is the vertical conductivity, w is the Darcy velocity of the brine (used for parameterizing rapid and slow modes of gravity-driven brine drainage; see A. Turner et al., 2013), and F represents the external energy flux to the ice (from atmosphere or ocean). The (bulk) salinity of the ice ($S = \phi S_{br}$) is a prognostic variable, and is computed as

$$\frac{\partial(\phi S_{br})}{\partial t} = w\frac{\partial S_{br}}{\partial z} + G \ , \tag{3}$$

where G is a sink term modeling slow drainage of brine from ice (see A. Turner et al., 2013). Inclusion of prognostic salinity into ice thermodynamics requires modifications in the calculation of the ice thermal conductivity, basal growth rate, frazil growth rate, rate of snow-to-ice conversion, and melt pond flushing (see A. Turner & Hunke, 2015). Compared to constant-salinity sea ice thermodynamics (see Bitz & Lipscomb, 1999), mushy layer thermodynamics augments both frazil and snow-to-ice growth: ice growth over open water occurs more readily with less heat loss to the atmosphere, as new ice is represented as an amalgam of solid ice and brine; and conversion of snow to ice is greater, as the thickness of the newly formed ice is reckoned to be that of the seawater-flooded snow, not compacted snow (A. Turner & Hunke, 2015).

Antarctic sea ice seasonal climatology and variability in CESM2 are evaluated over the final 600 years of a 1100-year preindustrial run, where the atmospheric CO_2 concentration is fixed at 280 ppm and all other atmospheric constituents are held at preindustrial levels (see Danabasoglu et al., 2019). All model components are (nominally) at 1^o spatial resolution. Sea ice seasonal climatology and variability in CESM2 is compared to that over years 1100 to 1700 of the CESM1 Large Ensemble preindustrial run (Kay et al., 2015). In order to assess the impact of mushy layer thermodynamics on the Antarctic ice pack in CESM2, we also make use of a 50-year pre-industrial simulation performed with a version of CESM2 where CICE5 uses the older Bitz and Lipscomb (1999) constant salinity sea ice thermodynamics scheme (as described in Bailey et al., 2020, submitted, referred to hereafter as CESM2-BL99); CESM2 and CESM2-BL99 configurations are identical in nearly all other respects (see Supplemental Information, SI, for further details).

It is not necessarily appropriate (or useful) to compare CESM2 and CESM1 pre-industrial control experiments directly with observations over the satellite era, as present-day sea ice conditions have been subject to a variety of modern-day forcings, including greenhouse gases and stratospheric ozone depletion over the South pole, which were not present in the pre-industrial climate. However, where reasonable, we compare Antarctic sea ice climatologies from CESM2 and CESM1 preindustrial experiments with observations of Antarctic sea ice area from 1979 to 2018, collected through passive microwave satellite retrieval and processed through NASA Team and Bootstrap algorithms (Cavalieri et al., 1996, updated yearly, 1999; Comiso & Nishio, 2008).

3 Results

We begin by comparing the seasonal cycle in monthly mean Antarctic sea ice area in CESM2, CESM1, and satellite observations from 1979 to 2018 (Fig 1). Overall, both models agree on the phasing of the sea ice seasonal cycle, and closely follow that of the satellite era observations. In both models and in observations, Antarctic sea ice area is minimal in February and maximal in September (Fig 1a). The sea ice growth season extends from March through August, while the melt season is from October through January; sea ice growth and melt, however, do occur year-round regionally in both CESM2 and CESM1, as we describe further below.

CESM2 has significantly less Antarctic sea ice area than CESM1 year-round: September sea ice area is approximately 1.5 million km^2 lower in CESM2 (15.9 million km^2 in CESM2 compared to 17.4 million km^2 in CESM1), while February sea ice area is approximately 1.0 million km^2 lower (2.7 million km^2 in CESM2 versus 3.7 million km^2 in CESM1). Though CESM2 has considerably less sea ice area than CESM1, sea ice area observed over the satellite era (1979 to 2018) is still approximately a half a million to a million km^2 less than that in CESM2 in the annual mean (Fig 1a, compare blue and cyan lines and with solid black line; Antarctic sea ice area in the NASA Team-processed satellite observations are approximately 0.4 million km^2 less than that in CESM2 in the annual mean, while ice area in the Bootstrap-processed observations are approximately 1.0 million km^2 less than that in CESM2 in the annual mean). Greater sea ice area in CESM2 relative to satellite era observations may either reflect systematic biases in CESM2, or reflect the very different forcings present over the late 20th and early 21st centuries, compared to those imposed in the CESM2 pre-industrial experiment. Indeed, historical CESM2 runs evince much closer agreement between modelled sea ice area and observations (DuVivier et al., 2019, submitted). Comparison of historical runs of state-of-the-art models participating in the sixth Climate Model Intercomparison Project (CMIP6) show that CESM2 is one of few in which both February and September sea ice extent are within range of those observed over the satellite era (only 7 models out of 40 showed such agreement; see Roach et al., 2020).

We compare interannual variability in the sea ice seasonal cycle between CESM2, CESM1, and satellite-era observations by comparing their standard deviations in monthly sea ice area (Fig 1b). In general, CESM2 has less variability in monthly sea ice area than CESM1, particularly from April to November, encompassing the mid- to late- growth season and early melt season (Fig 1b, compare solid and dotted black lines). We further assess the variability in monthly mean sea ice area in the two models by computing the monthly sea ice area standard deviation in the models using all contiguous 40-year segments sampled from each pre-industrial control experiment, and comparing the envelope of these standard deviations (Fig 1b, dark grey and light grey shaded regions show the standard deviation range in CESM2 and CESM1, respectively) to the monthly standard deviations in sea ice area from the last 39 years of the observations (Fig 1b, solid blue and cyan lines). Over much of the seasonal cycle, the monthly sea ice area standard deviation in the observations falls within (or nearly within) the range of that in both models. However, the variability in the observations substantially exceeds that in both models in the middle of the melt season (November and December; compare shaded grey regions to blue line in Fig 1b), suggesting that both models may have too little interannual variability in the hemispheric total sea ice area at this time of year.

In Figure 2, we compare sea ice area and extent between CESM2 and CESM1, focusing on the annual, summer (December, January, and February average; DJF), and winter (June, July, and August average; JJA) means. Reduced sea ice area and extent in CESM2, relative to CESM1, is evident over most sectors and seasons around the continent, particularly the Ross Sea, Weddell Sea, and southern Indian Ocean; only the Amundsen-Bellinghausen sector shows slightly greater sea ice extent in CESM2 compared to CESM1, especially in winter (JJA; compare Figs 2g and h, and difference in Fig 2i). In summer (DJF), decreased sea ice area and extent in CESM2 is evident around the whole continent, as the sea ice edge retreats substantially further towards the Antarctic coast in CESM2 compared to CESM1 (compare Figs 2d and e, and difference in Fig 2f).

Differences between CESM2 and CESM1 are also evident in the interannual variability of the location of the ice edge (Fig 2, dashed red lines). In both CESM2 and CESM1, interannual variability in the ice edge is greatest over the West Antarctic sectors, particularly the Weddell and Amundsen-Bellinghausen Seas in summer (Figs 2d and e) and winter (Figs 2g and h). In summer, there is greater interannual variability in the location of the sea ice edge over the Ross and Weddell sectors of the West Antarctic in CESM2, relative to CESM1. At the same time, there is somewhat less interannual variability in the location of the ice edge over East Antarctic sectors in the CESM1, relative to CESM2 (Figs 2d and e).

In addition to having reduced area and extent, Antarctic sea ice is also somewhat thinner in CESM2 than CESM1 (Fig 3, colors): circumpolar annual mean sea ice thickness is 0.76 m in CESM2, compared to 0.78 m in CESM1. Thinner sea ice in CESM2 may possibly bring modeled ice thickness closer to that in present-day observations, reckoned to be 0.62 ± 0.67 m for level ice in the annual mean (from shipboard observations collected in the Antarctic Sea ice Process and Climate, ASPeCt, dataset; see Worby et al., 2008), though ice thickness for both models lies well within the uncertainty range of these observations. Moreover, ice thickness differences between the models vary greatly between regional sectors. Year-round, the icepack in CESM2 is significantly thinner in the Ross and (coastal) Amundsen-Bellinghausen sectors, relative to CESM1 (red shading in Figs 3c, f, i), but somewhat thicker in the Weddell and East Antarctic (Indian and West Pacific) sectors. Because sea ice is (on average) slightly thinner and significantly less extensive in CESM2, there is less ice volume in CESM2 relative to CESM1 (13.8×10^3 km^3 in CESM2 compared to 14.6×10^3 km^3 in CESM1).

We also note substantial regional heterogeneity in Antarctic sea ice thickness over the course of the seasonal cycle, which also differs in some respects between the two models. In both models, sea ice is thinnest over the East Antarctic sectors year-round, and thickest over the West Antarctic: ice is thickest in the Amundsen, Bellinghausen, and Ross seas in CESM1 (Fig 3a), and in the Amundsen and western Weddell seas in CESM2 (Fig 3b). In CESM1, sea ice remains thick over the Amundsen-Bellinghausen sector in summer (Fig 3e), and also thickens over the Ross and Weddell sectors in winter (Fig 3g). In CESM2, on the other hand, ice remains thick over the Amundsen and eastern Weddell Seas in summer (Fig 3e), and also thickens over the Bellinghausen, western Weddell, and Ross Seas in winter (Fig 3h). Thick ice also hugs much of the Antarctic coast in CESM2, even in summer (Fig 3e). These regions of thicker coastal sea ice (reminiscent of land-fast sea ice, though CICE5 does not have a land-fast sea ice parameterization) are particularly evident over the East Antarctic in CESM2 in summer, but are notably absent in CESM1 (compare Figs 3d and e, and difference in 3f).

Thinner sea ice in CESM2 also corresponds to warmer surface skin temperatures over the ice pack (compare the 260K isotherm in Figs 3a and b; also note differences in Fig 3c). In summer, surface skin temperatures over much of the ice pack are at least 1K warmer in CESM2 relative to CESM1 (Fig 3f), and a substantial portion of the ice pack in CESM2 reaches the melting temperature (between 271K and 273K, depending on the brine concentration of the ice). In CESM2, the 270K isotherm follows the Antarctic coast over nearly all sectors (except the Weddell; see Fig 3e); in CESM1, on the other hand, the 270K isotherm is distant from the coast, particularly over West Antarctic sectors (Fig 3d), indicating that much of the ice pack over this region never reaches the melting temperature at the surface. In winter, surface temperatures are also greater in CESM2 than CESM1 (compare Figs 3g and h, and differences in 3i), which may occur because thinner sea ice has a greater equilibrium radiative temperature at its top surface than thicker ice, all other factors being equal (see Thorndike, 1992; Leppäranta, 1993). Moreover, global mean surface temperatures are approximately 1.2K warmer in CESM2 than CESM1 year-round, which may also partly account for warmer surface temperatures over sea ice in CESM2.

The seasonal cycle of hemispheric total ice growth and melt also differs substantially between CESM2 and CESM1. The sea ice model (CICE5 in CESM2 and CICE4 in CESM1) computes thermodynamic and dynamic changes in ice thickness in separate modules; changes in ice volume due to individual thermodynamic growth (basal, frazil, and snow-to-ice) and melt (top, basal, and lateral) processes are calculated separately and archived by the model, and the sum of these respective growth and melt terms is shown in Figure 4. In general, the rates of ice growth and melt are larger in CESM2 than CESM1 (Fig 4, compare solid and dotted lines), indicating that the sea ice annual cycle is more intense in CESM2 than CESM1. In both models, ice grows most rapidly during the growth season (March through August) and melts most rapidly during the melt season (October through January); however, ice growth also occurs during the melt season, and ice melt also occurs during the growth season, albeit at slower rates. The rate of sea ice growth in CESM2 exceeds the rate of sea ice growth in CESM1 year-round by up to 50%, with the largest differences between the two models occurring in the late growth season and early melt season (August to November, with the largest percentage differences in October and November; Fig 4, compare indigo lines). The rate of sea ice melt is also greater in CESM2 over the growth season and the early melt season (April through November); however, the rate of ice melt in CESM1 exceeds that in CESM2 in the late melt season (January and February; Fig 4, compare red lines), possibly because there is substantially more sea ice available to melt in CESM1 than in CESM2 at this point in time.

As described earlier in §2, the most significant difference between the sea ice formulations in the CICE5 (in CESM2) versus the CICE4 (in CESM1) is the mushy-layer thermodynamics in the former, which has supplanted the BL99 thermodynamics in the latter. However, neither the thinner ice pack nor the less extensive sea ice area in CESM2, compared to CESM1, is directly attributable to differences in sea ice thermodynamics; comparative studies of both thermodynamic formulations employed in the same sea ice model, with all other model components being identical, suggest that the mushy-layer formulation tends to thicken sea ice and increase the extent of the ice pack (A. Turner & Hunke, 2015; Bailey et al., 2020, submitted), which is opposite the differences we find between CESM2 and CESM1. In the following sections, we further explore how differences in sea ice growth and melt, partly attributable to these different formulations of sea ice thermodynamics, interact with different atmospheric and oceanic factors in these two models to produce the distinct Antarctic sea ice climatologies reported here.

3.1 Sea Ice Growth

We now consider differences between sea ice growth in CESM2 versus CESM1 in greater detail. The CICE model simulates three types of sea ice growth (Hunke & Lipscomb, 2008): frazil (open-water) growth, where sea ice forms over open water as ocean mixed layer temperatures drop below the freezing point; basal (congelation) growth, where sea ice growth at the bottom surface of the ice is driven by conductive fluxes through the ice; and snow-to-ice growth, where snow is converted to ice when the weight of overlying snow depresses the top surface of the ice below the sea surface. Total sea ice growth, dh/dt_{growth}, is due to the sum of basal, frazil, and snow-to-ice growth components:

$$\left(\frac{dh}{dt}\right)_{growth} = \left(\frac{dh}{dt}\right)_{basal} + \left(\frac{dh}{dt}\right)_{frazil} + \left(\frac{dh}{dt}\right)_{snow} . \tag{4}$$

Figure 5 shows the relative contributions of frazil, basal, and snow-to-ice terms in monthly mean sea ice growth in CESM2 and CESM1. While basal growth is weaker in CESM2 than CESM1, frazil and snow-to-ice growth are more vigorous. Greater snow-to-ice and frazil growth, and decreased basal growth, are also found when mushy-layer thermodynamics replaces BL99 in CICE5 within the fully-coupled CESM2 (CESM2-BL99; also see §2, Supplemental Information, SI, and Bailey et al., 2020, submitted), suggesting that differences between CESM2 and CESM1 in the relative contributions of these sea ice growth terms can be attributed, at least in part, to their different thermodynamic formulations (mushy-layer in CESM2/CICE5 versus BL99 in CESM1/CICE4).

Indeed, the magnitude and seasonality of each of the sea ice growth terms in CESM2-BL99 is very similar to corresponding terms in CESM1 (see SI Fig S1; compare dash-dot lines to respective dotted lines), not CESM2, suggesting that the relative prevalence of different ice growth modalities strongly depends on the sea ice thermodynamics formulation. Furthermore, other relevant factors that may impact ice growth are similar between CESM2 and CESM2-BL99, indicating that these factors cannot be responsible for differences in growth. Sea ice thickness, for example, impacts snow-to-ice growth: thicker ice requires a greater mass of snow to depress the ice surface below the freeboard and initiate conversion of accumulated snow to ice. However, the Antarctic ice pack in CESM2 and CESM2-BL99 is of similar thickness (see SI Fig S2), suggesting that this factor cannot account for greater snow-to-ice conversion. Similarly, snowfall over the ice pack is nearly indistinguishable between CESM2 and CESM2-BL99 (see SI Fig S3), suggesting that differences in snow accumulation over sea ice are also not responsible for differences in snow-to-ice conversion rates between the two. Finally, the surface wind stress in CESM2 and CESM2-BL99 is very similar (see SI Fig S4), indicating that greater frazil ice growth in CESM2 is unlikely to be due to greater sea ice divergence. Taken together, these lines of evidence indicate that it is the mushy layer thermodynamics formulation that augments frazil and snow-to-ice growth in CESM2 relative to CESM1, not differences in ice thickness, snowfall over the ice pack, or surface wind stress. In other words, replacing BL99 thermodynamics with mushy layer thermodynamics is sufficient to augment frazil and snow-to-ice growth, and decrease basal growth, even as other characteristics of the ice pack (such as thickness), snowfall over ice, and surface wind stress, remain unchanged.

We now examine each sea ice growth term in further detail. The frazil (open-water) sea ice growth rate is approximately twice as large in CESM2 as in CESM1 (Fig 5, compare solid and dotted teal lines), and the peak in frazil ice formation occurs slightly later in the growth season in CESM2 (April in CESM1 versus May in CESM2). Greater frazil growth is facilitated by mushy-layer thermodynamics, as a brine-ice slurry can be formed with less latent heat exchange, compared to that required when ice salinity is assumed constant (A. Turner & Hunke, 2015). The spatial distribution of frazil sea ice growth also differs between CESM2 and CESM1 (compare Figs 6a, d, g with Figs 7a, d, g). While frazil growth can occur within the ice pack itself, particularly early in the season when the sea ice fraction is lower (see Figs 6a, 7a), most frazil growth occurs near the Antarctic coast in both models. However, coastal frazil growth is at least two to four times more vigorous in CESM2 than CESM1 throughout the growth season, especially over West Antarctic sectors. Frazil growth in CESM2-BL99 more closely resembles that in CESM1, not CESM2, indicating that the introduction of the mushy layer thermodynamics formulation in CESM2 is sufficient to instigate vigorous open-water ice formation off the coast (compare Fig S5a, d, e with Figs 6a, d, e and 7a, d, e).

Greater coastal frazil growth in CESM2 is especially significant in light of *in situ* observations of Antarctic sea ice formation in winter, which document vigorous ice production of several meters (m^3 per m^2) per year within coastal polynyas around the Antarctic continent (Tamura et al., 2008, 2016). Such coastal latent heat polynyas are driven by katabatic (down-slope) winds off the Antarctic continent, which elicit large turbulent fluxes from the ocean mixed layer, and advect newly-formed sea ice away from the coast to expose more open water for further open-water sea ice growth (reviewed by Maqueda et al., 2004). While the spatial distribution of polynyas in CESM2 agrees well with those reported by Tamura et al. (2016), the CESM2 has notably weak polynya activity in the Ross sector and over the West Antarctic peninsula compared to observations.

Furthermore, buoyancy loss in these coastal polynyas, through both surface heat loss and brine rejection from newly-formed sea ice, supports formation of Antarctic Bottom Water (AABW), the most dense water in the world ocean (Goosse et al., 1997; Ohshima et al., 2013). More vigorous frazil ice formation in coastal polynyas in CESM2 relative to CESM1 hints at differences in AABW formation between the two models. Preliminary analysis of ocean salinity under ice suggests that the vertical salinity gradient is significantly greater in CESM2 than CESM1 (see SI, Fig S6). Further exploration of such differences is warranted (but beyond the scope of the present study).

In both models, basal (congelation) growth is the largest contributor to sea ice thickening over much of the growth season. The basal growth rate is approximately 25% smaller in CESM2 than CESM1 throughout the growth season (Fig 5, compare solid and dotted turquoise lines), and the peak in basal growth is approximately one month later in CESM1 than CESM2 (June in CESM1 versus May in CESM2). The spatial distribution of basal growth is similar in both models: greatest near the Antarctic coast, particularly over the East Antarctic sectors, and smallest near the ice edge (Figs 6b, e, h and Figs 7b, e, h). Basal growth is comparable in magnitude between both models at the beginning of the growth season (compare Fig 6b with Fig 7b), but declines much more in the mid- and late- growth season in CESM2 than CESM1 (compare Figs 6e, h with Figs 7e, h). Less basal growth in CESM2 compared to CESM1 is likely attributable to their different sea ice thermodynamics formulations: CESM2-BL99 has a basal growth rate similar to CESM1, not CESM2 (see SI, Fig S1). As we show later in §3.3, decreased basal growth in CESM2 is also consistent with greater ocean heat convergence under the ice pack in this model, compared to CESM1.

As basal growth declines in the mid- to late- growth season in both models, snow-to-ice growth increases, peaking at the ice area maximum in September, and persisting through the early melt season (Fig 5, purple lines). Observations of sea ice growth in the Antarctic suggest that snow-to-ice growth is particularly important in this hemisphere (Jeffries et al., 2001; Maksym & Markus, 2008): the Antarctic ice pack is thinner than that of the Arctic, and snowfall is more plentiful because of the adjacent storm track, making snow-to-ice growth an important component of the sea ice budget (Eicken, 2003). Antarctic snow-to-ice growth is nearly twice as large in CESM2 relative to CESM1, and the greater ice growth rate in CESM2 in the mid- to late- growth season and early melt season is entirely attributable to this term (recall Fig 4a). Unlike basal and frazil growth, which occur at the coast and at the center of the ice pack, snow-to-ice growth occurs near the edge of the ice pack in both models (compare Figs 6c, f, i to Figs 7c, f, i).

Significantly greater snow-to-ice growth in CESM2 is due, at least in part, to mushy-layer thermodynamics: because the mushy-layer formulation allows prognostic salinity within the ice, seawater flooding of snow layers is permitted as the weight of snow depresses ice below the water line, and the resulting ice growth is assessed to be the full depth of the flooded snow (i.e. snow plus brine; see A. Turner & Hunke, 2015). In the BL99 formulation, on the other hand, snow-to-ice growth is weaker because it is assumed that snow must be compressed to produce ice, thereby decreasing the thickness of ice that can be formed from the same quantity of snow. Indeed, the magnitude and seasonality of snow-to-ice growth in CESM2-BL99 resembles that in CESM1, not CESM2, suggesting that mushy layer thermodynamics plays an important role in augmenting conversion of accumulated snow to ice.

Somewhat thinner ice in CESM2 may also permit greater snow-to-ice growth, as less snow is required to depress the surface of the ice below the water line (recall Fig 3). However, we note that the winter sea ice pack is only thinner over some Antarctic sectors in CESM2 (recall Fig 3i), but snow-to-ice growth is greater over all sectors (compare Figs 6c, f, i with Figs 7c, f, i), suggesting that thinner ice is not the primary factor responsible for greater snow-to-ice growth in CESM2. Moreover, snow-to-ice growth in CESM2-BL99 resembles that in CESM1, not CESM2 (recall Fig S1; also compare Figs S5c, f, i with Figs 6c, f, i and 7c, f, i), even though ice thickness is very similar between CESM2-BL99 and CESM2 (recall Fig S2), further indicating that differences in ice thickness are not primarily responsible for differences in snow-to-ice conversion rates.

Additionally, as shown in Figure 8, greater snow-to-ice growth in CESM2 may also occur because of greater snowfall year-round over the ice pack. While there is greater snowfall equatorward of the ice edge in winter and spring in CESM1 (Fig 8, brown colors north of the ice edge), there is greater snowfall poleward of the ice edge year-round in CESM2 (green colors south of the ice edge; note that only differences in June and July are statistically significant at $p < 0.05$). The latter increase permits more snow accumulation near the edge of the ice pack in CESM2, and this snow is more readily converted to ice. Indeed, there is less snow depth over sea ice in CESM2 than CESM1 (not shown) though snowfall is greater, indicating more ready snow-to-ice formation in the former than in the latter.

3.1.1 Relationships Between Sea Ice Growth Processes

We now consider relationships between frazil, basal, and snow-to-ice growth terms, as evaluated from lead-lag correlations between the area-integrated monthly mean value of each term with every other term (as shown in Fig 9). We find many similarities, but also significant differences, between these relationships in CESM2 compared to CESM1, suggesting that mechanisms driving interannual variability in sea ice growth (and, therefore, ice area, extent, and volume) likely differ between the two models.

We begin with the relationship between basal and frazil growth, which differs markedly between the two models (compare Figs 9a and b). In CESM1, greater frazil growth over the growth season (February through September) is strongly correlated with greater basal growth over concurrent and subsequent months (Fig 9a, red region). Conditions that favor frazil growth (such as strong upward turbulent and net radiative fluxes from surface to atmosphere) also favor basal growth, so the close correspondence between these two growth terms at zero lead-lag (i.e. concurrently) is unsurprising. Furthermore, frazil growth earlier in the season may be necessary for subsequent basal growth later in the season, as frazil growth provides a 'platform' of thin ice on which basal growth can commence. While these reasonable relationships between frazil and basal growth are clearly evident in CESM1, they are nearly absent in CESM2 (compare Figs 9a and b). This may be due to weak basal growth in CESM2, relative to CESM1, which disrupts these expected correlations between frazil and basal growth terms. Further study of these growth relationships in both models is warranted.

The relationships between basal and snow-to-ice growth are more qualitatively similar between the two models, though some differences are evident (compare Figs 9c and d). In both CESM2 and CESM1, vigorous basal growth early in the growth season leads vigorous snow-to-ice growth later in the season (red regions in Figs 9c and d). This may occur because basal growth early in the growth season creates a base of ice on which snow can accumulate, facilitating snow-to-ice conversion later in the growth season. This relationship persists to the end of the growth season and the early melt season (through November) in CESM1, but tapers away in the late growth season (through August) in CESM2. While basal growth promotes subsequent snow-to-ice growth in both models, vigorous snow-to-ice growth in the mid- and late- growth season tends to inhibit concurrent and subsequent basal growth in both models (Figs 9c and d, blue regions). Snow-to-ice growth depends on snow cover, which insulates the top surface of the sea ice, thereby stymieing basal growth by decreasing the conductive flux through the ice (Powell et al., 2005). Furthermore, snow-to-ice growth will thicken the ice, which will also reduce the conductive flux through the ice and slow basal growth (Maykut & Untersteiner, 1971; Thorndike, 1992). Though the negative correlation between late-season snow-to-ice conversion and subsequent basal growth is present in both models, the relationship tapers away more rapidly in CESM2 than CESM1 (by September in CESM2, but persisting through December in CESM1).

The relationships between frazil growth and snow-to-ice growth are also qualitatively similar between the two models (Figs 9e, f). In both, greater frazil ice formation early in the growth season (February to April) tends to lead greater snow-to-ice growth later in the season (red regions in Figs 9e, f), though the relationship wanes more rapidly with lead time in CESM2 than CESM1. Later in the growth season, however, greater frazil ice formation is linked to less concurrent snow-to-ice growth (blue regions near the dashed grey line in Figs 9e, f). Significant frazil growth later in the growth season may be an indicator of a sluggish growth season, implying a more limited base on which snow-to-ice conversion can occur. This latter relationship is conjectural, and more exploration of this point may be warranted.

3.2 Sea Ice Melt

While sea ice growth differs substantively between CESM2 and CESM1, sea ice melt is more qualitatively similar (Fig 10). The CICE model simulates three types of sea ice melt: basal (occurring at the bottom of the ice), lateral (occurring on the lateral edge of the ice), and top (occurring at the top face of the ice). Melt is greatest during the melt season, but substantial melt also occurs during the growth season (recall Fig 4). In both models, more than 95% of melt year-round occurs through basal melt (Fig 10, red lines), with much smaller contributions from lateral and top melt during the mid- to late- melt season (November through February; purple and gold lines in Fig 10). This distribution of terms differs substantially from the melt budget in the Arctic, where top melt plays a much larger role (Andreas & Ackley, 1982).

In CESM2, basal melt is greater than that in CESM1 over much of the year, including over the growth season and the early melt season (March through November). Greater basal melt in CESM2 is consistent with mushy-layer thermodynamics in this model, as the melt pond flushing and gravity drainage formulations promote more vigorous basal melt (A. Turner & Hunke, 2015; Bailey et al., 2020, submitted). However, basal melt in CESM1 exceeds that in CESM2 in the mid- to late- melt season (January and February), which may occur because there is significantly more ice remaining to melt in CESM1 than CESM2 at this point in time.

3.3 Sea Ice Dynamics and Thermodynamics

We now consider the interplay between the thermodynamics of ice growth and melt, described in the previous sections, and coupling between the sea ice, atmosphere, and ocean. We begin by assessing the spatial pattern of changes in sea ice volume with time (i.e. the ice volume tendency), which is due to the sum of thermodynamic and dynamic terms:

$$\frac{dV}{dt} = \left(\frac{dV}{dt}\right)_{thermodynamics} + \left(\frac{dV}{dt}\right)_{dynamics}, \tag{5}$$

where the thermodynamic contribution to ice volume change, $dV/dt_{thermodynamics}$, is due to the growth (frazil, basal, and snow-to-ice) and melt (basal, lateral, and top) processes described previously; and the dynamic contribution, $dV/dt_{dynamics} = -\nabla \cdot (\vec{v}\, V)$, is due to advection and convergence by the local ice pack velocity $\vec{v}$ (Hunke & Lipscomb, 2008).

In Figure 11, we show the thermodynamic and dynamic contributions to the ice volume tendency in CESM2 and CESM1 over selected months spanning the seasonal cycle, highlighting the melt season (November and January) and the growth season (April and July). Overall, both models generally agree qualitatively regarding these thermodynamic and dynamic contributions to ice volume change, though important differences do exist, as we describe further below. Over the melt season (November and January; Figs 11a-d and 11e-h), there is a thermodynamic decrease in sea ice volume near the center and edge of the ice pack in both models (red regions in Fig 11a, b, e, f), driven primarily through basal melt (recall Fig 10). At the same time, there is a modest dynamic divergence of ice volume away from the coast (red regions in Figs 11c, d), and a modest dynamic convergence of ice volume near the ice edge (light blue regions near the black ice edge contour in Figs 11c, d). Dynamic divergence of ice away from the center of the ice pack during the melt season is slightly greater in CESM2 than CESM1 (compare Figs 11c and d), which may be a factor in promoting greater ice melt in this model, as ice melt occurs more readily near the edge of the ice pack than at the center.

Over the growth season (April and July; Figs 11i-l and 11m-p), ice volume increases through thermodynamic processes in both models (i.e. frazil, basal, and snow-to-ice growth, as described in §3.1; blue regions in Figs 11i, j, m, n), but also declines through melt at the ice edge (red regions near the black ice edge contour). At the same time, there is significant dynamic divergence of ice volume away from the coast and center of the ice pack in both CESM2 and CESM1 (red regions in Figs 11k, l, o, p), and dynamic convergence of ice towards the edge of the ice pack (blue regions near the black ice edge contour). Thus, over the course of the growth season, ice grows near the coast and the center of the ice pack, diverges away from these regions of growth, converges towards the edge of the ice pack, and melts at the ice edge.

Figure 12 highlights differences between CESM2 and CESM1 in the relative contributions of thermodynamic and dynamic processes to the ice volume tendency over selected months spanning the growth season (April, June, and August; shown as the difference between CESM2 and CESM1). First, we examine differences in the thermodynamic contributions to the ice volume tendency between CESM2 and CESM1 (Figs 12a, c, e). Over the course of the growth season, melt at the ice edge is significantly greater in CESM2 than CESM1 (red regions near the black ice edge contours). Greater melt at the ice edge in CESM2 is evident nearly everywhere, including the Weddell and Ross sectors of the West Antarctic, and much of the East Antarctic. The Amundsen-Bellinghausen sector is one of the only regions where melt at the ice edge is not significantly greater in CESM2 than CESM1, though greater melt even here is evident near the end of the growth season (August; Fig 12e).

There are also differences in the dynamic contribution to ice volume change between CESM2 and CESM1 (Figs 12b, d, f). First, there is greater dynamic divergence of sea ice away from the coast and the center of the ice pack in CESM2 throughout the growth season (red regions in Figs 12b, d, f). Greater ice divergence is evident around much of the continent, and is particularly pronounced over the East Antarctic sectors, the Weddell Sea, and the Amundsen-Bellinghausen Seas. Greater transport of sea ice away from the Antarctic coast in CESM2 may contribute to more vigorous frazil ice growth in coastal polynyas in this model (recall Figs 5, 6, and 7). At the same time that more ice diverges away from the Antarctic coast in CESM2, there is correspondingly greater dynamic convergence of sea ice towards the ice edge (blue regions near the black ice edge contours). Dynamic ice volume convergence near the ice edge in CESM2 is pronounced around nearly the entire continent over the course of the growth season, though it is weakest relative to CESM1 circa the Ross sector.

To better understand the mechanisms responsible for these differences in the ice volume tendency between CESM2 and CESM1, we first examine the sea level pressure in both models in Figure 13 (colors; shown for selected months spanning the growth season: April, June, and August). Both CESM2 and CESM1 exhibit a distinct tripole of low sea level pressure centers circling the Antarctic continent (as has been analyzed previously by Raphael, 2004, 2007): over the Amundsen-Bellinghausen sector, the south Indian sector, and the western south Pacific sector. These low pressure centers are significantly deeper in CESM2 than CESM1 (compare Figs 13b, d, f with 13a, c, e), indicating greater stationary wave activity in the former than the latter (Raphael, 2004). As a result, there is greater advection of sea ice by the cyclonic quasi-geostrophic near-surface flows that arise from these low pressure centers in CESM2 compared to CESM1 (compare arrows in Figs 13b, d, f with 13a, c, e; also see Raphael, 2007). Consequently, more sea ice is transported away from the center of the ice pack and towards its edges in CESM2, as suggested earlier by differences in the dynamic ice volume tendency in the two models (recall Fig 12).

Much stronger near-surface zonal winds accompany the stronger stationary wave activity in CESM2, as shown in Figure 14. Both surface easterlies and westerlies are stronger year-round in CESM2 relative to CESM1 (colors in Fig 14; near-surface zonal winds in CESM2 and CESM1 are shown by the blue solid and blue dotted contours, respectively), indicating greater surface wind stress in CESM2 than CESM1. Despite substantially stronger zonal winds in CESM2, the latitude of zero wind velocity (i.e. where easterlies transition to westerlies) is only slightly more equatorward in CESM2 than CESM1 (compare zero solid and dotted contours in Fig 14). As the meridional gradient in the zonal wind is greater in CESM2 than CESM1, there is greater wind stress curl over the ice pack and the Southern Ocean in the former than the latter.

Greater wind stress curl in CESM2 also implies greater wind-driven upwelling beneath the ice pack in this model, relative to CESM1. As waters at greater depth are warmer than near-surface waters at this latitude, greater upwelling results in greater heating by increased vertical advection (Fig 15, colors show the difference in heating by vertical motions between CESM2 and CESM1 in K/day). Greater heating by vertical upwelling in CESM2 is most evident directly below the mixed layer under the seasonal ice pack (i.e., between the minima and maxima of ice extent, delineated by the vertical turquoise lines, and below the green lines denoting the base of the mixed layer), and tends to decrease the stratification of the water column; as a consequence, the vertical distance between the 27.3 and 27.7 isopycnal contours is approximately 50m greater circa 65S in CESM2 than CESM1 (compare solid purple and dotted purple lines in Fig 15). Indeed, weaker stratification in CESM2 cannot be due to weaker buoyancy forcing by the sea ice seasonal cycle, as ice growth and melt in the CESM2 exceeds that in the CESM1 year-round (recall Fig 4). Greater heating by vertical advection is also evident in the mixed layer itself, circa 60S, which corresponds to the location of the mean ice edge near the middle and end of the ice growth season.

Stronger surface wind stress, greater wind stress curl, more heating by vertical advection, and weaker ocean stratification all contribute to greater ocean heat flux convergence in CESM2, relative to CESM1, as shown in Figure 16. The monthly ocean heat flux convergence in the mixed layer, Q, is calculated for both models as a residual from the month-to-month temperature tendency of the mixed layer, dT/dt, and the total surface heat flux, F_{sfc} (which includes ice-ocean heat exchange):

$$\rho_W c_p H_{ML} \frac{dT}{dt} = Q + F_{sfc} \; , \tag{6}$$

where ρ_W is the density of seawater, c_p is its heat capacity, and H_{ML} is the mixed layer depth (see Bitz et al., 2012).

Compared to CESM1, we find that the ocean heat flux convergence over the growth season is modestly greater under the ice pack and significantly greater at the ice edge in CESM2. Early in the growth season, there is significantly greater ocean heat flux convergence under the ice pack in CESM2 (April; Fig 16a), which persists to some extent over the course of the growth season (June through August; Figs 16b, c), and may limit basal growth (recall Fig 5) and sea ice thickness (recall Fig 3) in this model. In the mid- to late- growth season, greater ocean flux convergence is most evident at the ice edge in CESM2 (June and August; Figs 16b, c), and is responsible for greater melt here (recall the more negative thermodynamic ice volume tendency at the ice edge in CESM2 during the growth season, as shown in Figs 12a, c, e). Significantly, greater ocean heat flux convergence at the ice edge in CESM2 coincides with areas where the ice edge is more poleward in CESM2 relative to CESM1; this is particularly evident in the eastern Weddell, Indian, and the Ross sectors, and suggests that greater ocean heating may play an important role in limiting sea ice extent in these regions in CESM2. As greater wind stress and more intense stationary wave activity in CESM2 diverges ice away from the Antarctic coast and center of the ice pack, greater ocean heat flux convergence simultaneously limits ice thickness and extent by increasing the heat flux from ocean to ice, thereby augmenting basal melt.

4 Discussion

In this overview of Antarctic sea ice in the pre-industrial era in the new CESM2, we describe its seasonal cycle, modalities of growth and melt, and interactions with both atmosphere and ocean, relative to that in CESM1. Overall, we find substantial differences between the old and new models, some of which are attributable to differences in how sea ice thermodynamics is treated, and others that are due to differences in the climatologies of the atmosphere and ocean.

Treating sea ice as a mushy layer, an amalgam with varying amounts of solid ice and microscopic liquid brine inclusions, rather than as a solid with fixed salinity (as in BL99), has been shown to impact the seasonal cycle of sea ice in both hemispheres (A. Turner & Hunke, 2015; Bailey et al., 2020, submitted). We find that in CESM2, the new mushy-layer thermodynamics treatment changes the spatial and temporal distribution of the different modalities of Antarctic sea ice growth relative to CESM1. Both frazil (open water) ice formation and snow-to-ice conversion make substantially greater contributions to Antarctic ice growth in CESM2 than CESM1, while basal (congelation) growth makes a smaller contribution. Greater frazil ice growth in CESM2 is concentrated within Antarctic coastal polynyas, while greater snow-to-ice conversion occurs at the center and edge of the growing ice pack. Observational studies show that such frazil and snow-to-ice growth processes are crucial for Antarctic sea ice growth in the real world (see, e.g., Jeffries et al., 2001; Maqueda et al., 2004; Maksym & Markus, 2008; Tamura et al., 2008, 2016), and it is possible that improved representation of these processes in the new model implies better agreement with real-world observations. Further quantitative intercomparison between model results (particularly historical, rather than pre-industrial, experiments) and present-day *in situ* observations is needed.

While differing sea ice growth in CESM2 and CESM1 is attributable in part to the differing sea ice thermodynamic treatments in the two models, differing sea ice thickness and extent are more clearly linked to differing atmosphere and ocean dynamics. The extratropical atmospheric circulation in the Southern Hemisphere is more vigorous in CESM2 than CESM1, with more energetic stationary wave activity and surface winds. Deeper subpolar low pressure centers in CESM2 sweep sea ice away from the coast (helping facilitate frazil ice growth in coastal polynyas), increase sea ice divergence from the center of the ice pack, and drive sea ice equatorward. The latter tends to thin the ice pack, which is evident in the climatology of Antarctic sea ice in CESM2. On the other hand, sea ice area and extent are substantially lower in CESM2 than CESM1 as ocean heat flux convergence into the mixed layer is greater in the new model. Greater surface wind stress curl in CESM2 is responsible for more upwelling of warmer waters from depth, increasing ocean heating under and at the edge of the ice pack; previous studies have shown that such increased ocean heat flux convergence acts as a substantial control on ice extent in Earth system models (Bitz et al., 2005). Were it not for this greater ocean heat input at the edge of the ice pack, it is likely that Antarctic sea ice area would be more extensive in CESM2 than it is.

Our study highlights the need to consider a range of inter-related factors when comparing sea ice in global climate models with each other and with real-world observations. It is possible for two models to have similar sea ice area and volume, but to have a very different confluence of processes that maintain this climatology: an ice pack maintained by high wind stress and copious snowfall may appear very similar in volume and area to one maintained by cold temperatures and substantial basal growth, for example. The prevalent modes of sea ice growth and melt, the relationships between these modes, and the magnitude of the seasonal cycle are likely all of import in maintaining climatological ice area and volume. Similarly, winds, ocean hydrography, and heating (by both atmospheric and oceanic processes) also impact the ice pack. We suggest that it may be useful for model intercomparisons to consider more of these auxiliary factors when evaluating how well global climate models simulate sea ice. We also suggest that some of these auxiliary factors, if observable in the real world, could serve to constrain models in a more comprehensive manner beyond ice area and thickness.

These other climatological factors may also impact how Antarctic sea ice responds to increased atmospheric CO_2 and other climate forcing agents. Traditionally, the sensitivity of the ice pack to climate warming has often been described in terms of ice area and thickness, with thicker and more extensive sea ice shown to experience greater decline as the globe warms (see, for example, Holland & Bitz, 2003; Bitz & Roe, 2004). However, other factors may also be equally important, including modes of ice growth, the strength of stationary waves and zonal winds over the ice pack, and the intensity of the seasonal cycle. A decline in ice volume, for example, may occur because ice growth slows, but different modes of ice growth may not be equally sensitive to climate warming: basal growth may decline as warmer ocean waters and less heat loss from the ice top hinder efficient conduction through ice, but snow-to-ice conversion may increase if there is greater snowfall over the ice pack as the storm track shifts poleward. An ice pack that relies primarily on basal growth may be more sensitive to warming temperatures than one that relies more heavily on other modes of growth. As such, the relative sensitivity of the ice pack to warming may depend on climatological factors beyond ice area and volume. We suggest that consideration of such auxiliary factors may prove useful to further understanding of the mechanisms controlling the sensitivity of Antarctic sea ice to different anthropogenic forcings.

In this overview of Antarctic sea ice in the state-of-the-art CESM2, we have highlighted key differences in sea ice climatology and variability between the older CESM1 and the newer model. As Antarctic sea ice begins to retreat in response to a warming climate, Earth system models will continue to be an important tool for understanding the changing interplay between sea ice, ocean, and atmosphere in a warming world. CESM2, in conjunction with observations, reanalyses, and other Earth system models, will serve as an indispensable resource for understanding and anticipating these changes in Antarctic climate in the future.

5 Concluding Points

The major findings of this study can be summarized as follows:

- Antarctic sea ice is less extensive and slightly thinner in CESM2 compared to CESM1. Antarctic sea ice area in CESM2 more closely follows that in the satellite era observations, particularly in terms of maximum and minimum area.
- The seasonal cycle of Antarctic sea ice growth and melt are more intense in CESM2 than in CESM1.
- Mechanisms of sea ice growth in CESM2 differ substantially from those in CESM1: frazil and snow-to-ice growth are greater, and basal growth is weaker.
- Differences in sea ice growth between CESM2 and CESM1 are primarily due to the different sea ice thermodynamics schemes. Mushy layer thermodynamics, which

models prognostic salinity in the sea ice, increases snow-to-ice conversion and augments frazil (open-water) sea ice growth.

- Relationships between sea ice growth terms differ substantially between CESM2 and CESM1. Relationships are generally weaker in CESM2 than CESM1, particularly the link between early season frazil growth and later basal growth.
- During the growth season, there is greater stationary wave activity and greater westerly wind stress over the ice pack in CESM2, compared to CESM1. Stronger winds in CESM2 drive greater divergence of Antarctic sea ice away from the coast and center of the ice pack, and towards its edge.
- Greater wind stress curl over the ice pack in CESM2, relative to CESM1, drives more warm water upwelling. The resulting ocean heat flux convergence beneath the ice pack thins Antarctic sea ice in CESM2 and limits its extent.

Acknowledgments

All authors are grateful to three anonymous reviewers for their thoughtful feedback on an earlier version of the manuscript. LL was funded by NSF grant 1643484. The CESM project is supported primarily by the National Science Foundation (NSF). This material is based upon work supported by the National Center for Atmospheric Research (NCAR), which is a major facility sponsored by the NSF under Cooperative Agreement No. 1852977. Computing and data storage resources, including the Cheyenne supercomputer (doi:10.5065/D6RX99HX), were provided by the Computational and Information Systems Laboratory (CISL) at NCAR. CESM2 model output used in this study is available at the NCAR Digital Asset Services Hub (DASH; https://data.ucar.edu) as casename *b.e21.B1850.f09_g17.CMIP6-piControl.001*; CESM1 model output is available at the CESM Large Ensemble Community Project site (http://www.cesm.ucar.edu/projects/community-projects/LENS/) as casename *b.e11.B1850C5CN.f09_g16.005*.

References

Andreas, E., & Ackley, S. (1982). On the differences in ablation seasons of Arctic and Antarctic sea ice. *Journal of the Atmospheric Sciences*, *39*(2), 440–447.

Armour, K., Marshall, J., Scott, J., Donohoe, A., & Newsom, E. (2016, Jul). Southern Ocean warming delayed by circumpolar upwelling and equatorward transport. *Nature Geoscience*, *9*, 549-554.

Bailey, D., Holland, M., DuVivier, A., Hunke, E., & Turner, A. (2020, submitted).

Impact of sea ice thermodynamics in the CESM2 sea ice component. *Journal of Advances in Modeling Earth Systems*.

Beljaars, A., Brown, A., & Wood, N. (2004). A new parametrization of turbulent orographic form drag. *Quarterly Journal of the Royal Meteorological Society*, *130*(599), 1327–1347.

Bintanja, R., van Oldenborgh, G., Drijfhout, S. S., Wouters, B., & Katsman, C. (2013, Jul). Important role for ocean warming and increased ice-shelf melt in Antarctic sea ice expansion. *Nature Geoscience*, *6*, 376-379.

Bitz, C., Holland, M., Hunke, E., & Moritz, R. (2005, Aug). Maintenance of the sea ice edge. *Journal of Climate*, *18*, 2903-2921.

Bitz, C., & Lipscomb, W. (1999). An energy-conserving thermodynamic model of sea ice. *Journal of Geophysical Research: Oceans*, *104*(C7), 15669–15677.

Bitz, C., & Polvani, L. (2012). Antarctic climate response to stratospheric ozone depletion in a fine resolution ocean climate model. *Geophysical Research Letters*, *39*(L20705).

Bitz, C., & Roe, G. (2004). A mechanism for the high rate of sea ice thinning in the Arctic Ocean. *Journal of Climate*, *17*(18), 3623–3632.

Bitz, C., Shell, K., Gent, P., Bailey, D., Danabasoglu, G., Armour, K., … Kiehl, J. (2012). Climate sensitivity in the Community Climate System Model, version 4. *Journal of Climate*, *25*(9), 3053-70.

Blackport, R., & Kushner, P. (2017). Isolating the atmospheric circulation response to Arctic sea ice loss in the coupled climate system. *Journal of Climate*, *30*(6), 2163–2185.

Bogenschutz, P., Gettelman, A., Hannay, C., Larson, V., Neale, R., Craig, C., & Chen, C.-C. (2018). The path to CAM6: Coupled simulations with CAM5.4 and CAM5.5. *Geoscientific Model Development (Online)*, *11*(LLNL-JRNL-731418).

Cavalieri, D., Parkinson, C., Gloersen, P., Comiso, J., & Zwally, H. (1999). Deriving long-term time series of sea ice cover from satellite passive-microwave multisensor data sets. *Journal of Geophysical Research: Oceans*, *104*(C7), 15803–15814.

Cavalieri, D., Parkinson, C., Gloersen, P., & Zwally, H. (1996, updated yearly). *Sea ice concentrations from Nimbus-7 SMMR and DMSP SSM/I-SSMIS pas-*

sive microwave data, version 1. NASA National Snow and Ice Data Center Distributed Archive Center.

Comiso, J., & Nishio, F. (2008). Trends in the sea ice cover using enhanced and compatible AMSR-E, SSM/I, and SMMR data. *Journal of Geophysical Research: Oceans*, *113*(C2).

Danabasoglu, G., Bates, S. C., Briegleb, B. P., Jayne, S. R., Jochum, M., Large, W. G., ... Yeager, S. G. (2012). The CCSM4 ocean component. *Journal of Climate*, *25*(5), 1361–1389.

Danabasoglu, G., Lamarque, J.-F., Bacmeister, J., Bailey, D., DuVivier, A., Edwards, J., ... others (2019). The Community Earth System Model version 2 (CESM2). *Journal of Advances in Modeling Earth Systems*.

Deser, C., Tomas, R., & Sun, L. (2015, Mar). The role of ocean-atmosphere coupling in the zonal-mean atmospheric response to Arctic sea ice loss. *Journal of Climate*, *28*, 2168-2186.

DuVivier, A., Holland, M., Kay, J., Tilmes, S., Gettelman, A., & Bailey, D. (2019, submitted). Arctic and Antarctic sea ice state in the Community Earth System Model version 2. *Journal of Geophysical Research: Oceans*.

Eicken, H. (2003). Sea ice: an introduction to its physics, chemistry, biology and geology. In (p. 22-81). Wiley Online Library.

Eicken, H., Fischer, H., & Lemke, P. (1995). Effects of the snow cover on Antarctic sea ice and potential modulation of its response to climate change. *Annals of Glaciology*, *21*, 369–376.

England, M., Polvani, L., & Sun, L. (2018). Contrasting the Antarctic and Arctic atmospheric responses to projected sea ice loss in the late twenty-first century. *Journal of Climate*, *31*(16), 6353–6370.

Feltham, D., Untersteiner, N., Wettlaufer, J., & Worster, M. (2006). Sea ice is a mushy layer. *Geophysical Research Letters*, *33*(14).

Garrison, D., & Buck, K. (1989). The biota of Antarctic pack ice in the Weddell Sea and Antarctic Peninsula regions. *Polar Biology*, *10*(3), 211–219.

Gettelman, A., & Morrison, H. (2015). Advanced two-moment bulk microphysics for global models. Part I: Off-line tests and comparison with other schemes. *Journal of Climate*, *28*(3), 1268–1287.

Gettelman, A., Morrison, H., Santos, S., Bogenschutz, P., & Caldwell, P. (2015).

Advanced two-moment bulk microphysics for global models. Part II: Global model solutions and aerosol–cloud interactions. *Journal of Climate*, *28*(3), 1288–1307.

Goosse, H., Campin, J.-M., Fichefet, T., & Deleersnijder, E. (1997). Impact of sea-ice formation on the properties of Antarctic Bottom Water. *Annals of Glaciology*, *25*, 276–281.

Gordon, A. (1981). Seasonality of Southern Ocean sea ice. *Journal of Geophysical Research: Oceans*, *86*(C5), 4193–4197.

Guo, H., Golaz, J.-C., Donner, L., Wyman, B., Zhao, M., & Ginoux, P. (2015). CLUBB as a unified cloud parameterization: Opportunities and challenges. *Geophysical Research Letters*, *42*(11), 4540–4547.

Holland, M., & Bitz, C. (2003). Polar amplification of climate change in coupled models. *Climate Dynamics*, *21*, 221-232.

Holland, M., Landrum, L., Kostov, Y., & Marshall, J. (2017). Sensitivity of Antarctic sea ice to the Southern Annular Mode in coupled climate models. *Climate Dynamics*, *49*, 1813-1831.

Holland, M., Landrum, L., Raphael, M., & Kwok, R. (2018). The regional, seasonal, and lagged influence of the Amundsen Sea Low on Antarctic sea ice. *Geophysical Research Letters*, *45*(20), 11–227.

Hoose, C., Kristjánsson, J., Chen, J.-P., & Hazra, A. (2010). A classical-theory-based parameterization of heterogeneous ice nucleation by mineral dust, soot, and biological particles in a global climate model. *Journal of the Atmospheric Sciences*, *67*(8), 2483–2503.

Hunke, E., & Lipscomb, W. (2008). *CICE: the Los Alamos sea ice model, documentation and software, version 4.0* (Tech. Rep. No. LA-CC-06-012). Los Alamos National Laboratory.

Hunke, E., Lipscomb, W., Turner, A., Jeffery, N., & Elliott, S. (2015). *CICE: the Los Alamos sea ice model, documentation and software, version 5.1* (Tech. Rep. No. LA-CC-06-012). T-E Fluid Dynamics Group, Los Alamos National Laboratory.

Jeffries, M., Krouse, H., Hurst-Cushing, B., & Maksym, T. (2001). Snow-ice accretion and snow-cover depletion on Antarctic first-year sea-ice floes. *Annals of Glaciology*, *33*, 51–60.

Kay, J., Deser, C., Phillips, A., Mai, A., Hannay, C., Strand, G., … Vertenstein, M. (2015). The Community Earth System Model (CESM) Large Ensemble project: A community resource for studying climate change in the presence of internal climate variability. *Bulletin of the American Meteorological Society*, *96*, 1333-1349.

Kwok, R., & Comiso, J. (2002). Southern Ocean climate and sea ice anomalies associated with the Southern Oscillation. *Journal of Climate*, *15*(5), 487–501.

Landrum, L., Holland, M., Raphael, M., & Polvani, L. (2017). Stratospheric ozone depletion: An unlikely driver of the regional trends in Antarctic sea ice in austral fall in the late twentieth century. *Geophysical Research Letters*, *44*(21), 11–062.

Larson, V. (2017). CLUBB-SILHS: A parameterization of subgrid variability in the atmosphere. *arXiv preprint arXiv:1711.03675*.

Leppäranta, M. (1993). A review of analytical models of sea-ice growth. *Atmosphere-Ocean*, *31*(1), 123–138.

Maksym, T., & Markus, T. (2008). Antarctic sea ice thickness and snow-to-ice conversion from atmospheric reanalysis and passive microwave snow depth. *Journal of Geophysical Research: Oceans*, *113*(C2).

Maqueda, M. M., Willmott, A., & Biggs, N. (2004). Polynya dynamics: A review of observations and modeling. *Reviews of Geophysics*, *42*(1).

Massom, R., Eicken, H., Hass, C., Jeffries, M., Drinkwater, M., Sturm, M., … others (2001). Snow on Antarctic sea ice. *Reviews of Geophysics*, *39*(3), 413–445.

Massom, R., Scambos, T., Bennetts, L., Reid, P., Squire, V., & Stammerjohn, S. (2018). Antarctic ice shelf disintegration triggered by sea ice loss and ocean swell. *Nature*, *558*(7710), 383–389.

Maykut, G., & Untersteiner, N. (1971). Some results from a time-dependent thermodynamic model of sea ice. *Journal of Geophysical Research*, *76*(6), 1550–1575.

McGraw, M., & Barnes, E. (2016). Seasonal sensitivity of the eddy-driven jet to tropospheric heating in an idealized AGCM. *Journal of Climate*, *29*, 5223-5240.

Meehl, G., Arblaster, J., Bitz, C., Chung, C., & Teng, H. (2016). Antarctic sea-ice expansion between 2000 and 2014 driven by tropical Pacific decadal climate variability. *Nature Geoscience*, *9*(8), 590–595.

Morrison, A., Kay, J., Chepfer, H., Guzman, R., & Yettella, V. (2018). Isolating the liquid cloud response to recent arctic sea ice variability using spaceborne lidar observations. *Journal of Geophysical Research: Atmospheres*, *123*(1), 473–490.

Ohshima, K., Fukamachi, Y., Williams, G., Nihashi, S., Roquet, F., Kitade, Y., ... others (2013). Antarctic Bottom Water production by intense sea-ice formation in the Cape Darnley polynya. *Nature Geoscience*, *6*(3), 235–240.

Parkinson, C., & Cavalieri, D. (2012). Antarctic sea ice variability and trends, 1979-2010. *The Cryosphere*, *6*, 871-880.

Pauling, A., Bitz, C., Smith, I., & Langhorne, P. (2016). The response of the Southern Ocean and Antarctic sea ice to freshwater from ice shelves in an Earth System Model. *Journal of Climate*, *29*, 1655-1672.

Pellichero, V., Sallée, J.-B., Schmidtko, S., Roquet, F., & Charrassin, J.-B. (2017). The ocean mixed layer under Southern Ocean sea-ice: Seasonal cycle and forcing. *Journal of Geophysical Research: Oceans*, *122*(2), 1608–1633.

Perovich, D., Richter-Menge, J., Polashenski, C., Elder, B., Arbetter, T., & Brennick, O. (2014). Sea ice mass balance observations from the North Pole Environmental Observatory. *Geophysical Research Letters*, *41*(6), 2019–2025.

Powell, D., Markus, T., & Stössel, A. (2005). Effects of snow depth forcing on Southern Ocean sea ice simulations. *Journal of Geophysical Research: Oceans*, *110*(C6).

Raphael, M. (2004). A zonal wave 3 index for the Southern Hemisphere. *Geophysical Research Letters*, *31*(23).

Raphael, M. (2007). The influence of atmospheric zonal wave three on Antarctic sea ice variability. *Journal of Geophysical Research: Atmospheres*, *112*(D12).

Raphael, M., & Hobbs, W. (2014). The influence of the large-scale atmospheric circulation on Antarctic sea ice during ice advance and retreat seasons. *Geophysical Research Letters*, *41*(14), 5037–5045.

Roach, L. A., Dörr, J., Holmes, C. R., Massonnet, F., Blockley, E. W., Notz, D., ... others (2020). Antarctic sea ice area in CMIP6. *Geophysical Research Letters*, *47*(9), e2019GL086729.

Rothrock, D., Yu, Y., & Maykut, G. (1999). Thinning of the Arctic sea-ice cover. *Geophysical Research Letters*, *26*(23), 3469–3472.

Scinocca, J., & McFarlane, N. (2000). The parametrization of drag induced by stratified flow over anisotropic orography. *Quarterly Journal of the Royal Meteoro-*

logical Society, *126*(568), 2353–2393.

Shi, X., Liu, X., & Zhang, K. (2015). Effects of pre-existing ice crystals on cirrus clouds and comparison between different ice nucleation parameterizations with the community atmosphere model (CAM5). *Atmospheric Chemistry and Physics (Online)*, *15*(PNNL-SA-103838).

Sigmond, M., & Fyfe, J. (2010). Has the ozone hole contributed to increased Antarctic sea ice extent? *Geophysical Research Letters*, *37*(L18502).

Simpkins, G., Ciasto, L., Thompson, D., & England, M. (2012). Seasonal relationships between large-scale climate variability and Antarctic sea ice concentration. *Journal of Climate*, *25*(16), 5451–5469.

Singh, H., Garuba, O., & Rasch, P. (2018). How asymmetries between Arctic and Antarctic climate sensitivity are modified by the ocean. *Geophysical Research Letters*, *45*(23), 13-31.

Singh, H., Polvani, L., & Rasch, P. (2019). Antarctic sea ice expansion, driven by internal variability, in the presence of increasing atmospheric CO_2. *Geophysical Research Letters*(doi: 10.1029/2019GL083758).

Smith, D., Dunstone, N., Scaife, A., Fiedler, E., Copsey, D., & Hardiman, S. (2017). Atmospheric response to Arctic and Antarctic sea ice: The importance of ocean–atmosphere coupling and the background state. *Journal of Climate*, *30*(12), 4547–4565.

Swart, N., & Fyfe, J. (2013). The influence of recent Antarctic ice sheet retreat on simulated sea ice area trends. *Geophysical Research Letters*, *40*, 4328-4332.

Swart, N., Fyfe, J., Hawkins, E., Kay, J., & Jahn, A. (2015). Influence of internal variability on Arctic sea-ice trends. *Nature Climate Change*, *5*(2), 86.

Tamura, T., Ohshima, K., & Nihashi, S. (2008). Mapping of sea ice production for Antarctic coastal polynyas. *Geophysical Research Letters*, *35*(7).

Tamura, T., Ohshima, K. I., Fraser, A. D., & Williams, G. D. (2016). Sea ice production variability in Antarctic coastal polynyas. *Journal of Geophysical Research: Oceans*, *121*(5), 2967-2979. Retrieved from `https://agupubs.onlinelibrary.wiley.com/doi/abs/10.1002/2015JC011537` doi: 10.1002/2015JC011537

Thorndike, A. (1992). A toy model linking atmospheric thermal radiation and sea ice growth. *Journal of Geophysical Research*, *97*(C6), 9401-9410.

Turner, A., & Hunke, E. (2015). Impacts of a mushy-layer thermodynamic approach in global sea-ice simulations using the CICE sea-ice model. *Journal of Geophysical Research: Oceans*, *120*(2), 1253–1275.

Turner, A., Hunke, E., & Bitz, C. (2013). Two modes of sea-ice gravity drainage: A parameterization for large-scale modeling. *Journal of Geophysical Research: Oceans*, *118*(5), 2279–2294.

Turner, J., Comiso, J., Marshall, G., Lachlan-Cope, T., Bracegirdle, T., Maksym, T., ... Orr, A. (2009). Non-annular atmospheric circulation change induced by stratospheric ozone depletion and its role in the recent increase in Antarctic sea ice extent. *Geophysical Research Letters*, *36*(L08502).

Vancoppenolle, M., Fichefet, T., & Goosse, H. (2009). Simulating the mass balance and salinity of Arctic and Antarctic sea ice. 2. importance of sea ice salinity variations. *Ocean Modelling*, *27*(1-2), 54–69.

Wall, C., Kohyama, T., & Hartmann, D. (2017). Low-cloud, boundary layer, and sea ice interactions over the Southern Ocean during winter. *Journal of Climate*, *30*, 4857-4871.

Wang, Y., Liu, X., Hoose, C., & Wang, B. (2014). Different contact angle distributions for heterogeneous ice nucleation in the Community Atmospheric Model version 5. *Atmospheric Chemistry and Physics*, *14*(19), 10411–10411.

Worby, A. P., Geiger, C. A., Paget, M. J., Van Woert, M. L., Ackley, S. F., & DeLiberty, T. L. (2008). Thickness distribution of Antarctic sea ice. *Journal of Geophysical Research: Oceans*, *113*(C5). Retrieved from `https://agupubs.onlinelibrary.wiley.com/doi/abs/10.1029/2007JC004254` doi: 10.1029/2007JC004254

Zhang, L., Delworth, T., Cooke, W., & Yang, X. (2019). Natural variability of Southern Ocean convection as a driver of observed climate trends. *Nature Climate Change*, *9*(1), 59.

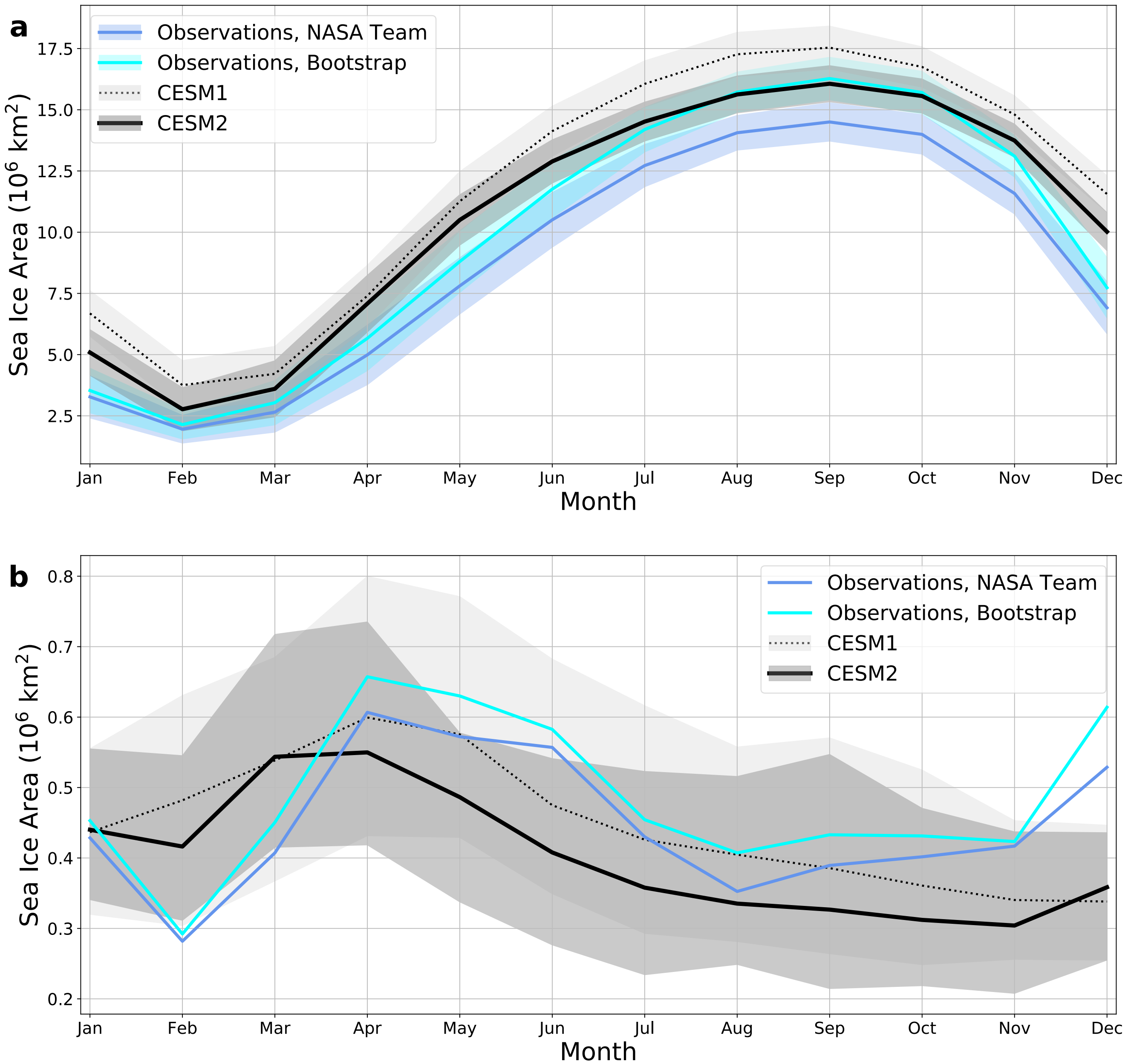

Figure 1. Seasonal Cycle of Sea Ice Area: (a) Monthly mean sea ice area, and (b) one standard deviation of the monthly sea ice area, both in 10^6 km^2. Shown for CESM2 (black, solid), CESM1 (black, dotted), and the satellite observations from 1979 to 2018 (blue and cyan). Shading in (a) provides the two standard deviation envelope for the variability in monthly ice area, while shading in (b) gives the range of the monthly standard deviation in each model, calculated for all contiguous 40-yr time periods in each 600-year pre-industrial run.

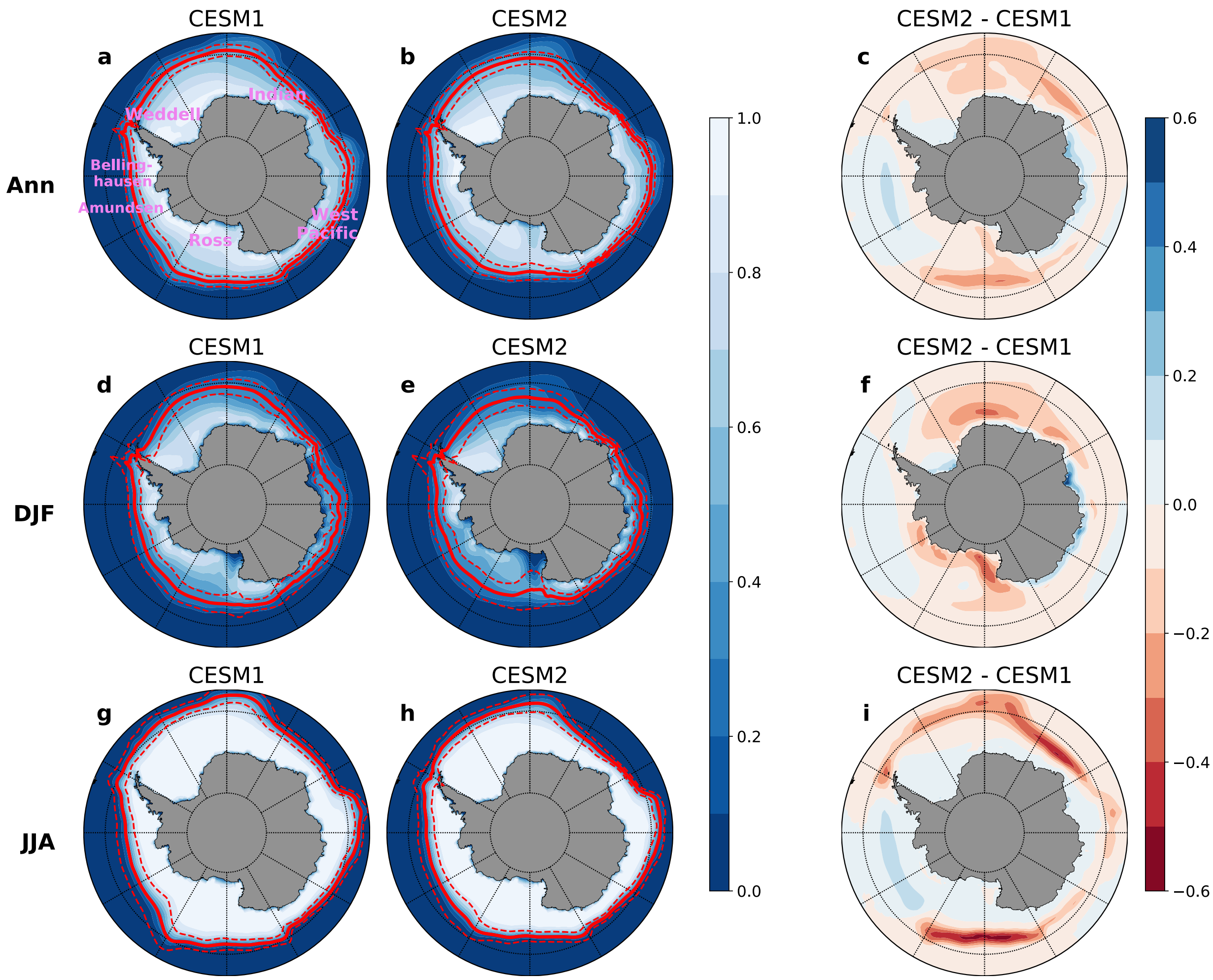

Figure 2. Ice Fraction and Extent: Sea ice fraction (colors) and sea ice extent (the 0.15 ice fraction isoline; thick red contour) in (a, d, g) CESM1 and (b, e, h) CESM2; panels (c, f, i) show the difference in sea ice fraction between CESM2 and CESM1 (colors). Shown for (a, b, c) the annual mean, (c, d, e) the December-January-February (DJF) mean, and (g, h, i) the June-July-August (JJA) mean. In the left and center columns, the dashed red contours show the one-standard-deviation envelope of the ice extent. Panel (a) indicates the sectors of the Antarctic referred to in the main text.

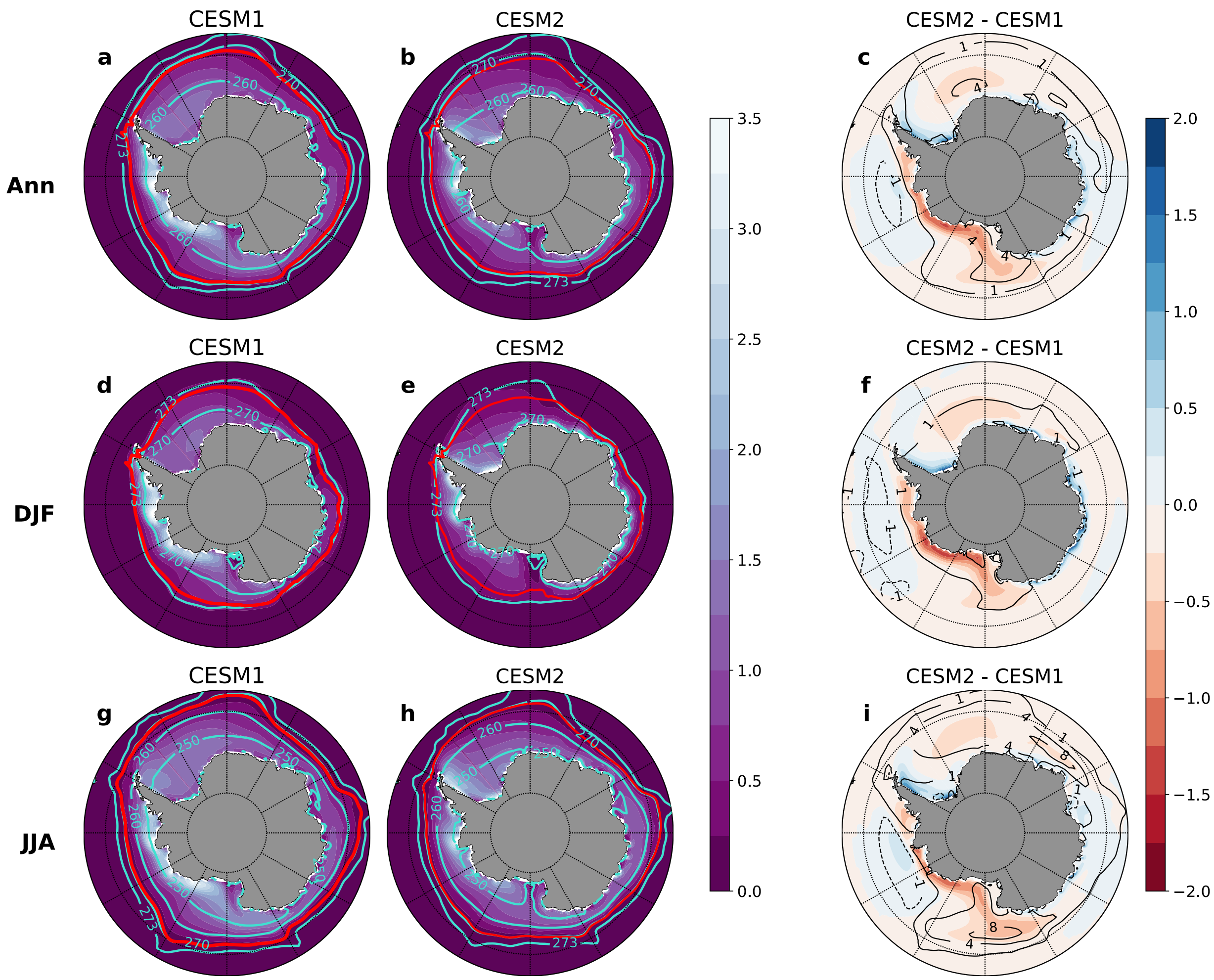

Figure 3. Ice Thickness and Surface Temperature: Sea ice thickness (in m; colors) and surface skin temperature (turquoise contours at [250, 260, 270, 273] K) in (a, e, h) CESM1 and (b, f, i) CESM2; panels (c, g, j) show differences between the CESM2 and CESM1 (temperature differences shown as black contours at [-1, 1, 4, 8] K; colors indicate ice thickness differences in m). Shown for (a, b, c) the annual mean, (d, e, f) the December-January-February (DJF) mean, and (g, h, i) the June-July-August (JJA) mean. In the left and center columns, the red contour shows the 0.15 ice fraction isoline.

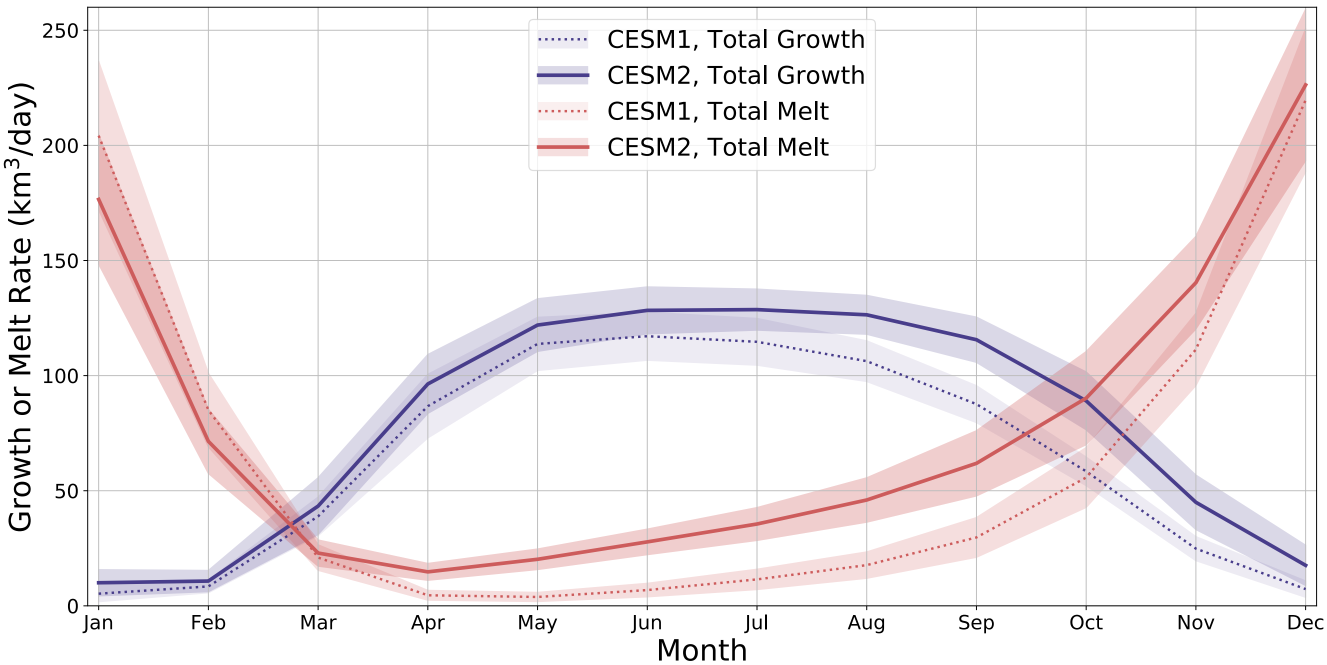

Figure 4. Antarctic Sea Ice Growth and Melt Rates: Monthly mean total sea ice growth rate (indigo lines) and melt rate (red lines) over the Antarctic in CESM2 (solid lines) and CESM1 (dotted lines), in km^3/day. Shaded envelopes show the one-standard-deviation range over each month in each model.

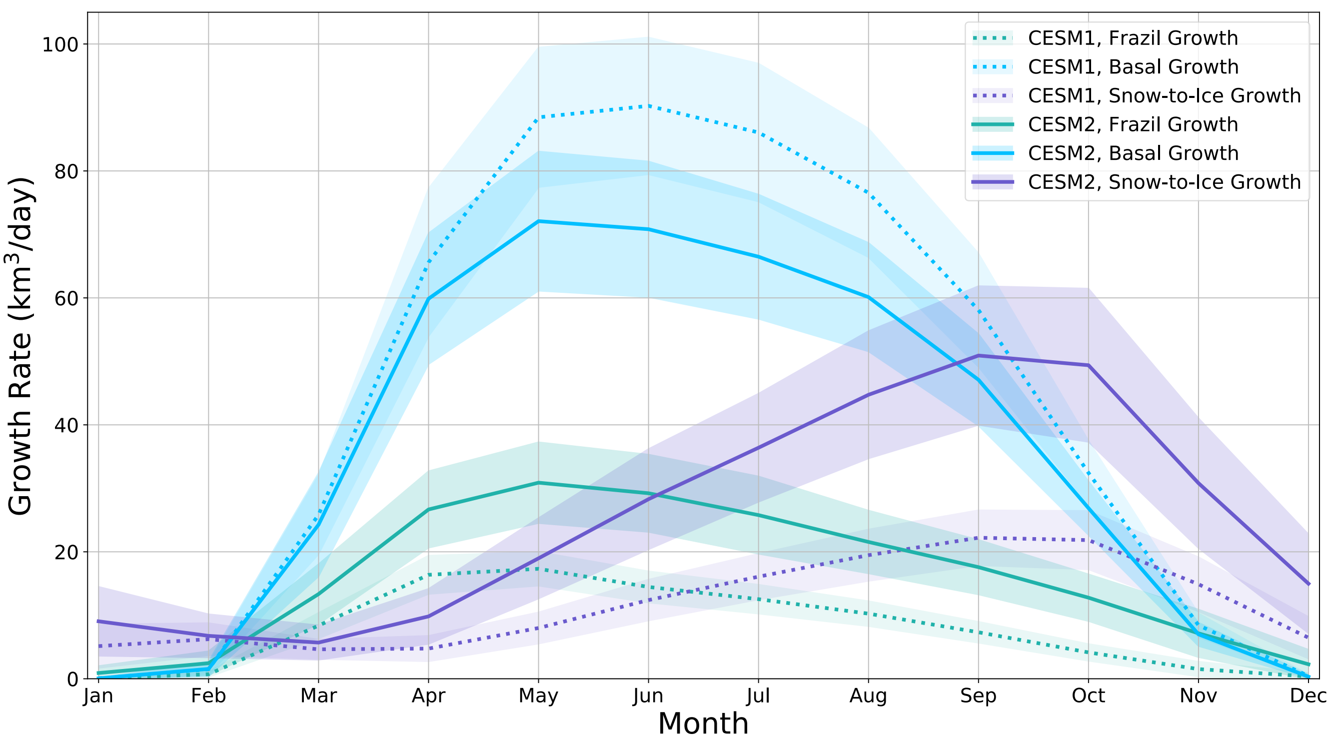

Figure 5. Components of Antarctic Sea Ice Growth: Monthly mean frazil growth (teal lines), basal growth (turquoise lines), and snow-to-ice growth (purple lines) in CESM2 (solid lines) and CESM1 (dotted lines), in km^3/day. Shaded envelopes show the one-standard-deviation range for each month and each model.

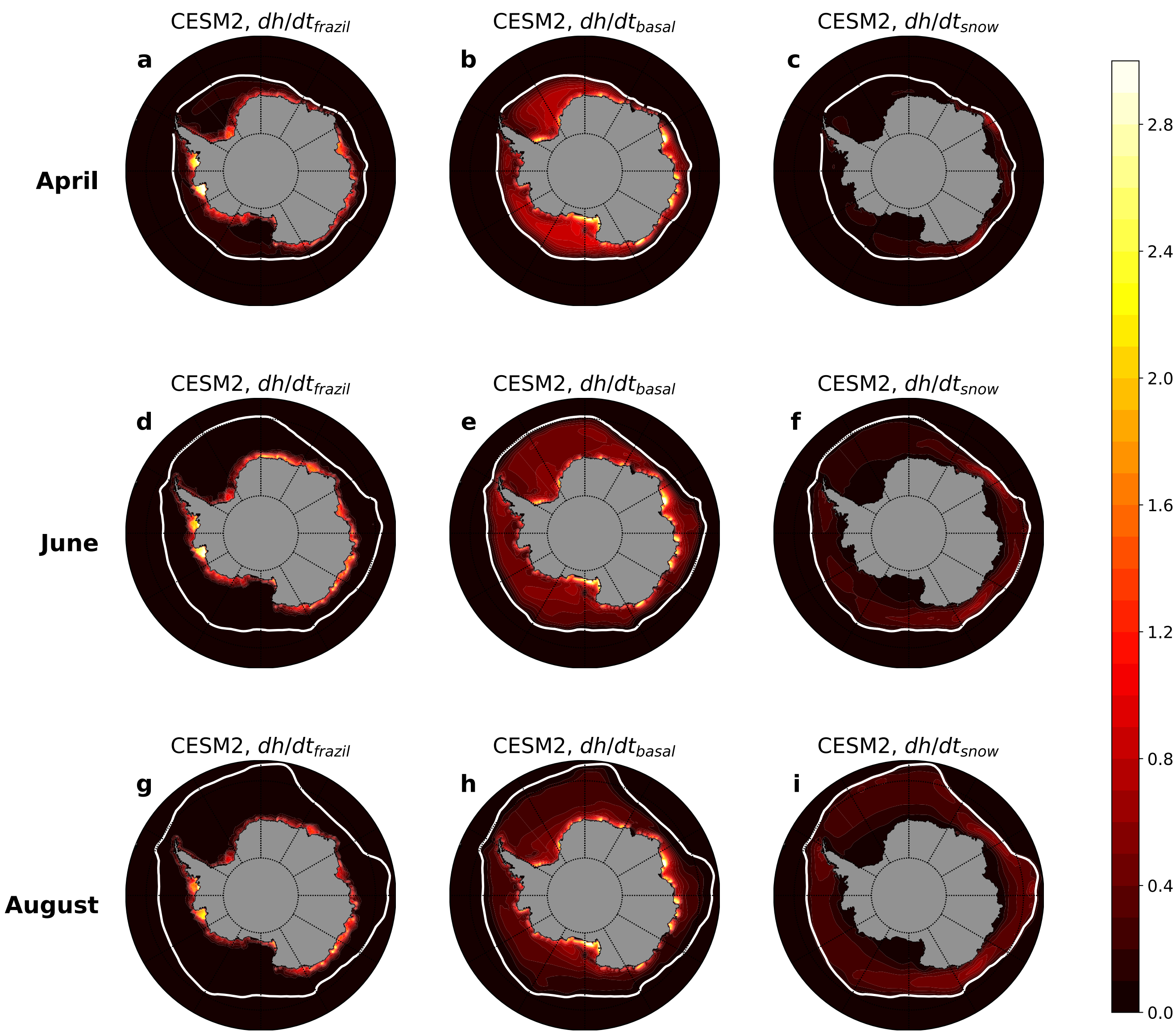

Figure 6. Antarctic Sea Ice Growth in CESM2: Monthly mean (a, d, g) frazil growth, (b, e, h) basal growth, and (c, f, i) snow-to-ice growth in (a, b, c) April, (d, e, f) June, and (g, h, i) August, in cm/day. In all panels, the white contour shows the 0.15 ice fraction isoline.

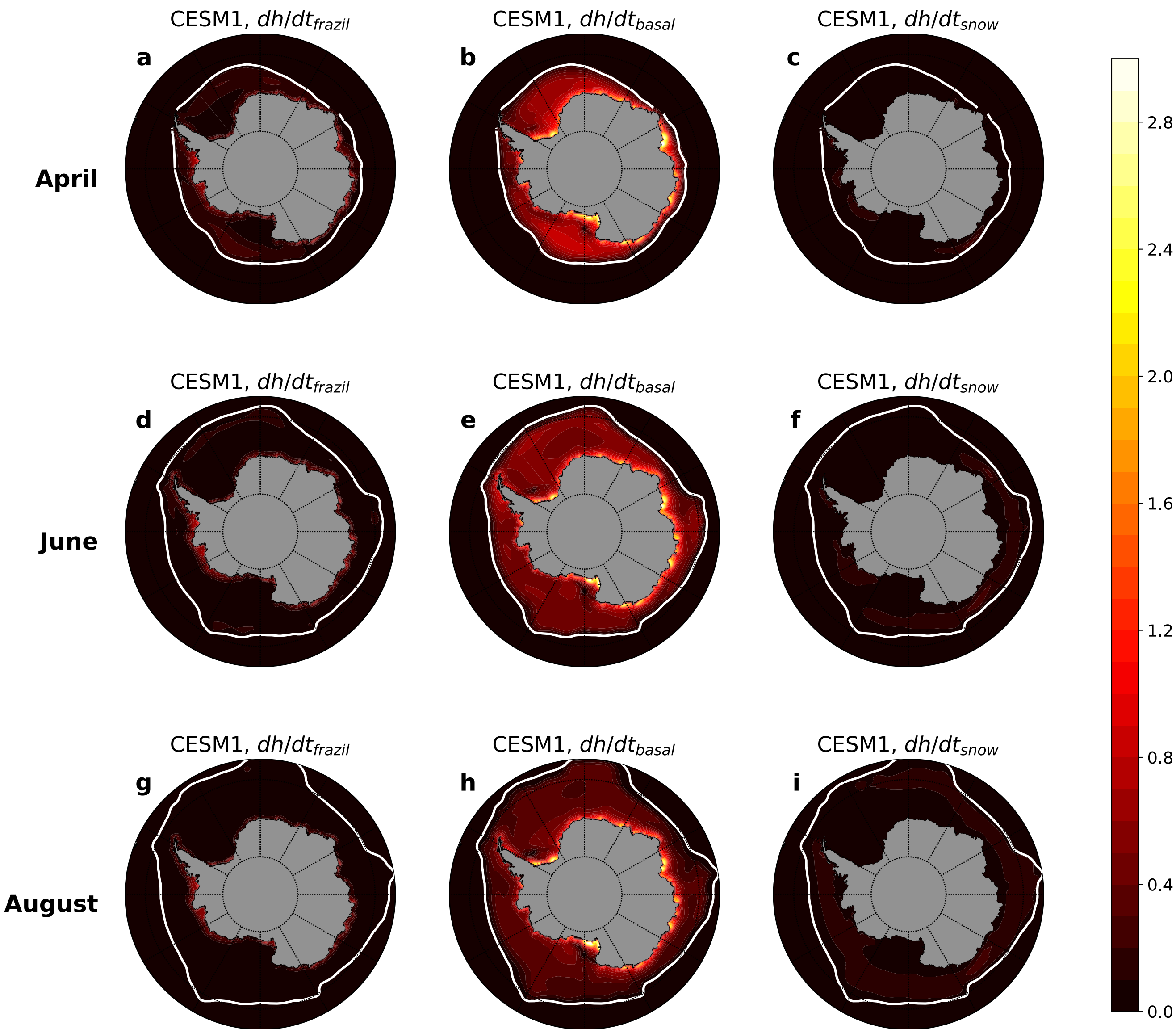

Figure 7. Antarctic Sea Ice Growth in CESM1: As in Fig 6, but for CESM1.

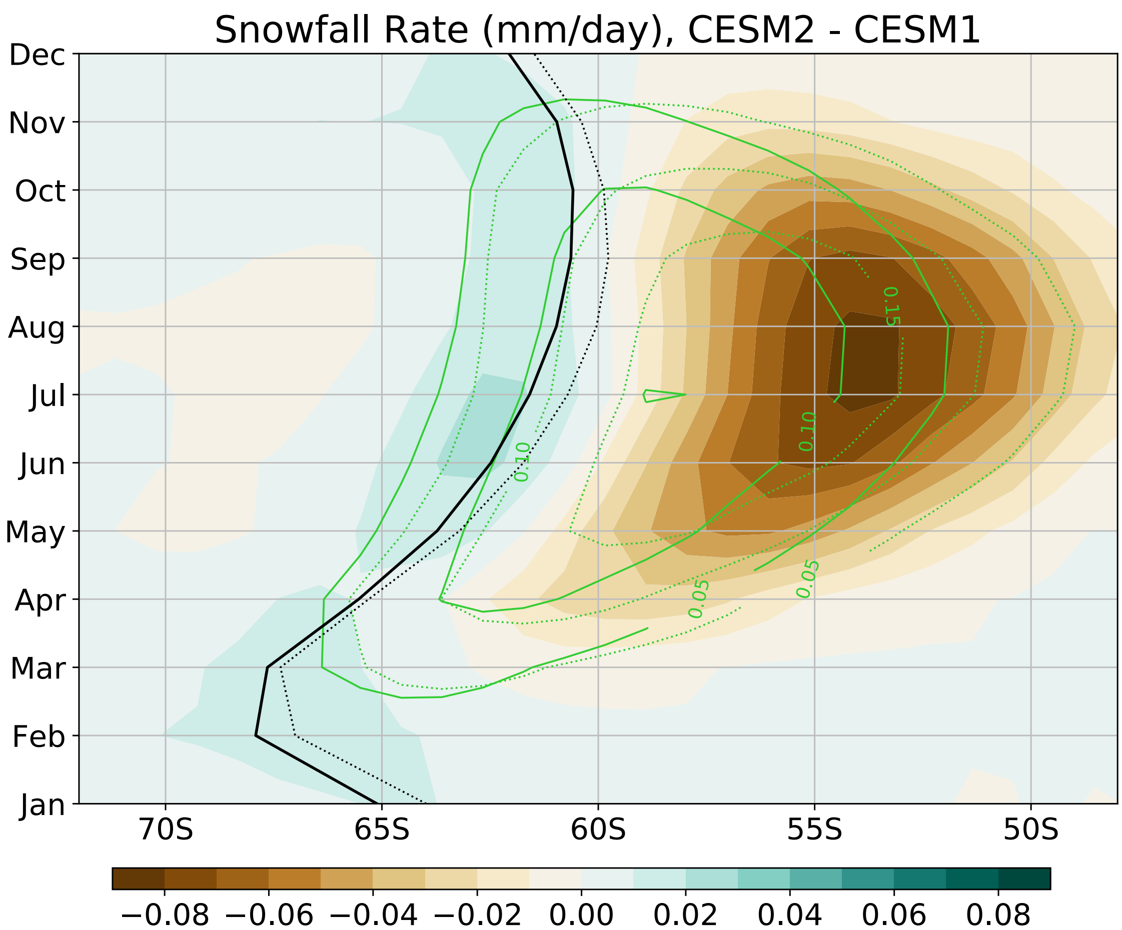

Figure 8. Zonal Mean Monthly Snowfall Rate: Difference between the monthly zonal mean snowfall rate in CESM2 and CESM1 (in mm/day; colors). Green solid and dotted contours (at 0.05, 0.1, and 0.15 mm/day) show the monthly zonal mean snowfall rates in CESM2 and CESM1, respectively. The monthly zonal mean ice extent (0.15 ice fraction isoline) for CESM2 (CESM1) is indicated by the solid (dotted) black contour.

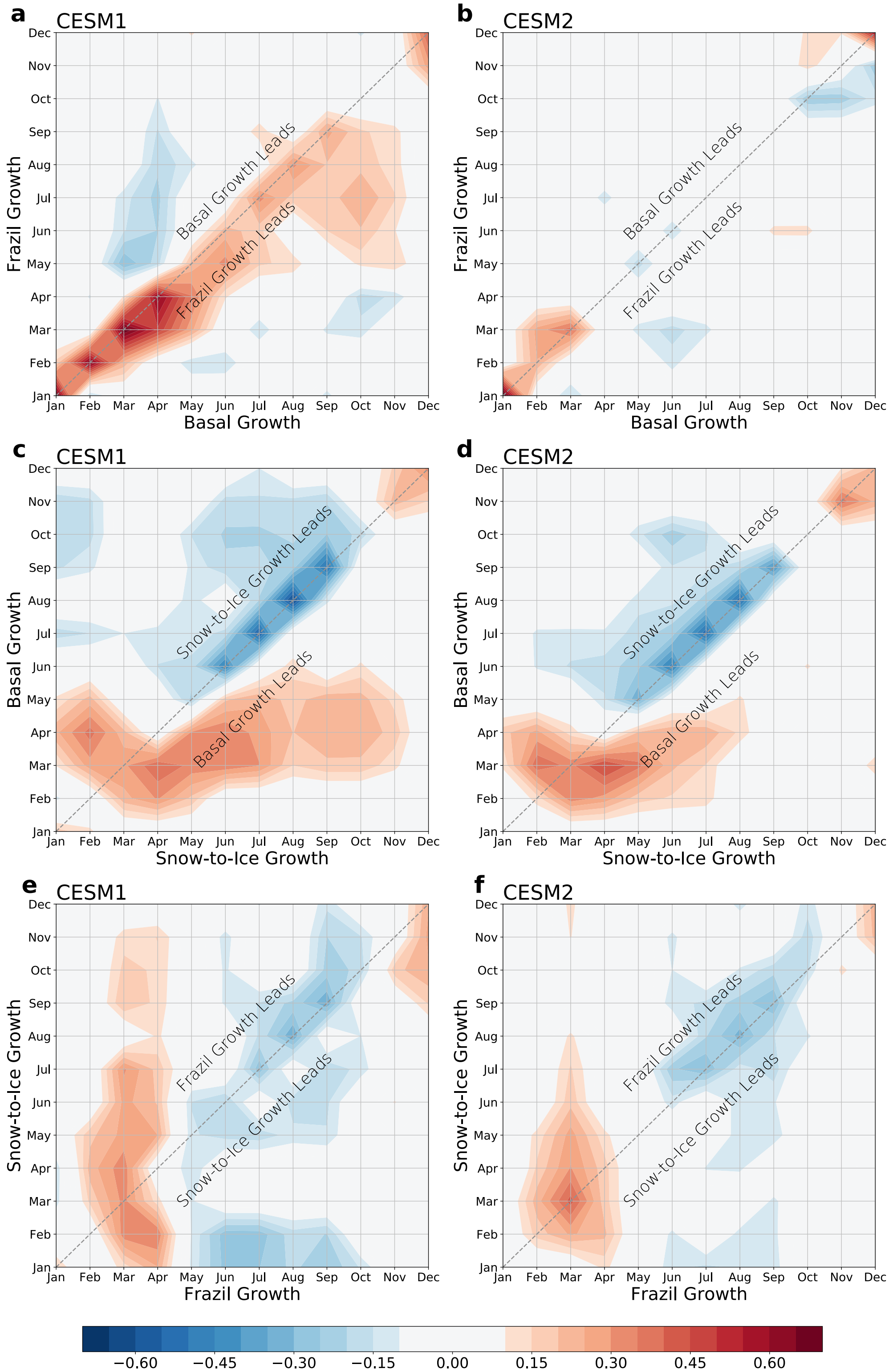

Figure 9. Relationships Between Sea Ice Growth Terms: Monthly lead-lag correlations between (a, b) frazil and basal growth, (c, d) basal and snow-to-ice growth, and (e, f) snow-to-ice and frazil growth in the (a, c, e) CESM1 and (b, d, f) CESM2. Only correlations that are statistically significant at $p < 0.05$ are shown.

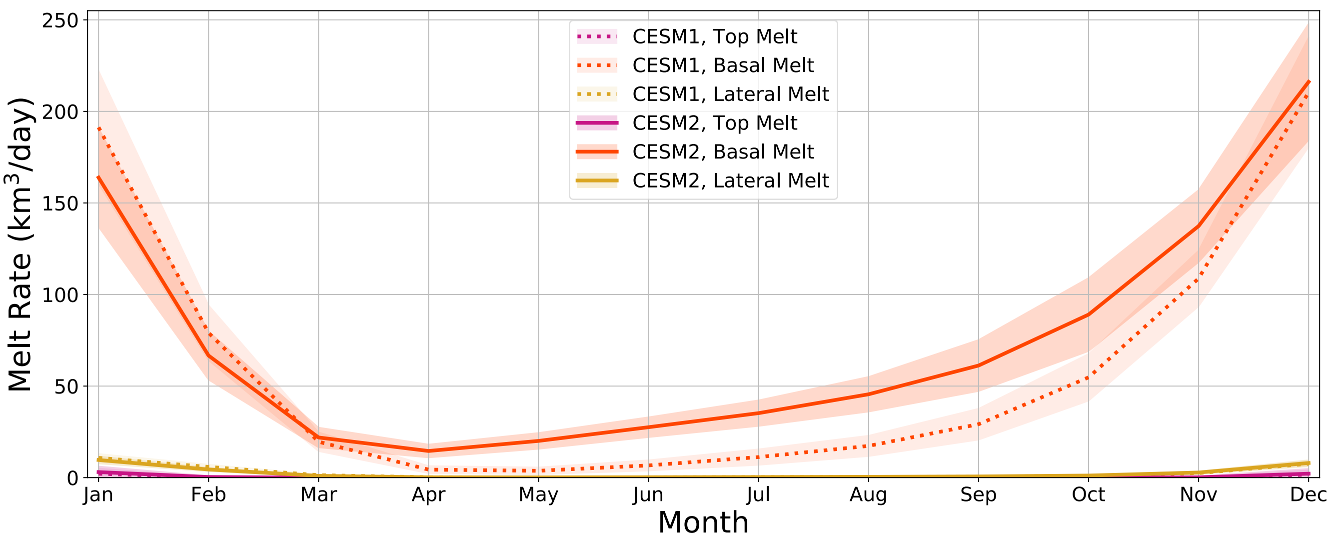

Figure 10. Components of Antarctic Sea Ice Melt: Monthly mean basal melt (red lines), lateral melt (gold lines), and top melt (purple lines) in CESM2 (solid lines) and CESM1 (dotted lines), in km^3/day. Shaded envelopes show the one-standard-deviation range in the melt term for each month and each model.

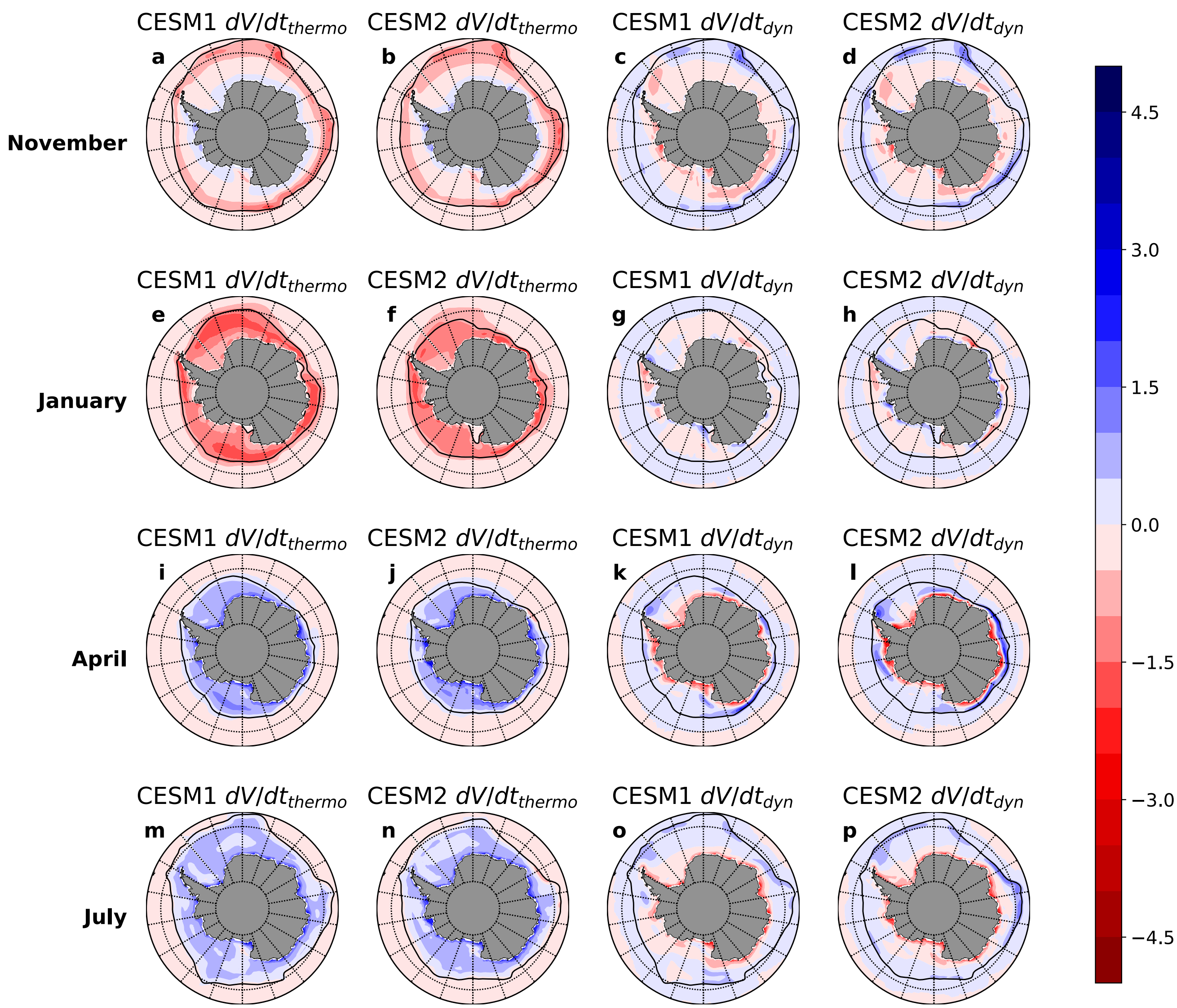

Figure 11. Thermodynamic and Dynamic Contributions to Antarctic Sea Ice Volume Change: Monthly mean (a, b, e, f, i, j, m, n) thermodynamic and (c, d, g, h, k, l, o, p) dynamic contributions to ice volume tendency dV/dt, in cm/day, in the (a, c, e, g, i, k, m, o) CESM1, and (b, d, f, h, j, l, n, p) CESM2. Shown for (a-d) November, (e-h) January, (i-l) April, and (m-p) July. In all panels, the black contour indicates sea ice extent (i.e. 0.15 ice fraction line).

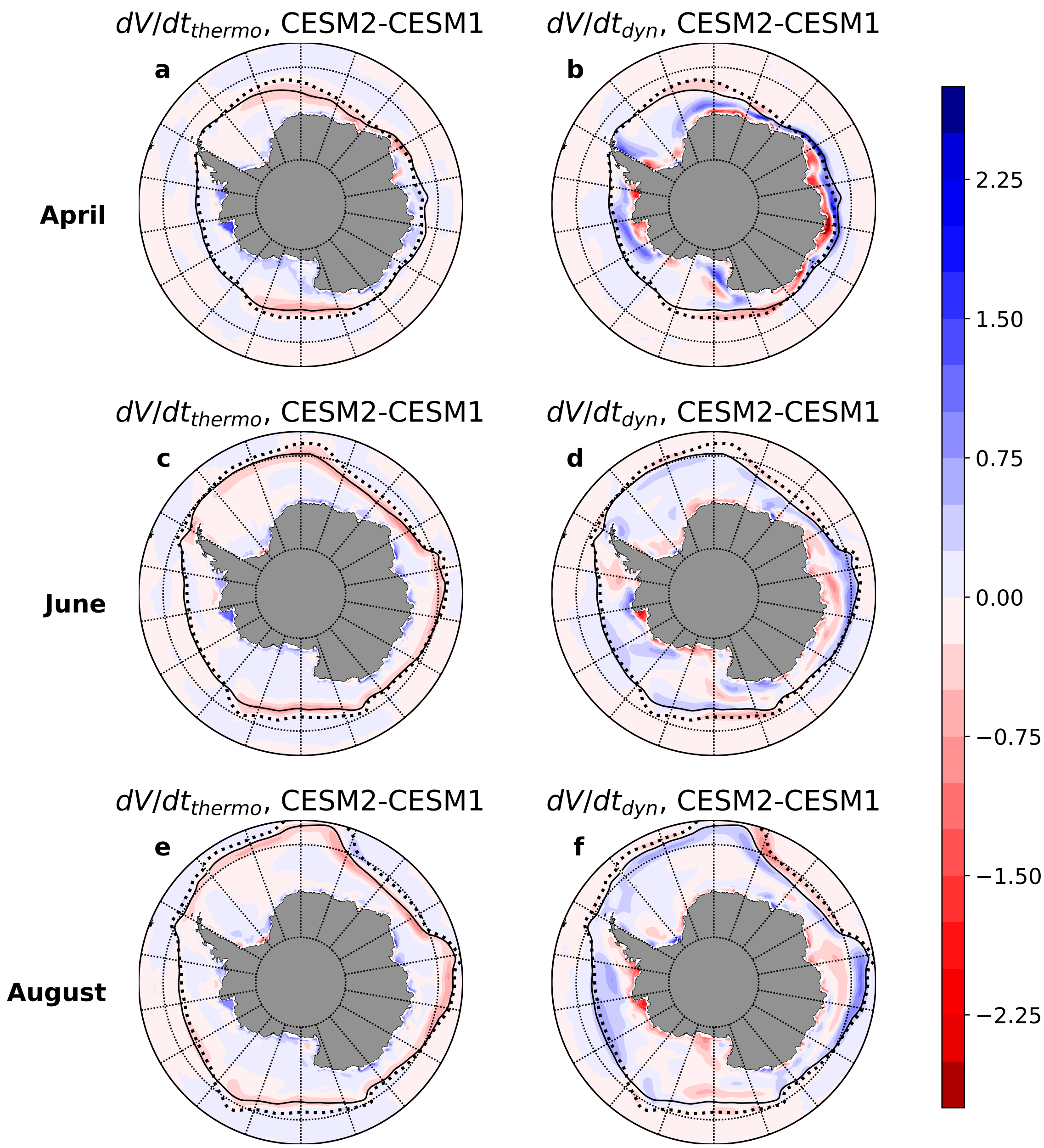

Figure 12. Differences in Thermodynamic and Dynamic Contributions to Antarctic Sea Ice Volume Change over the Growth Season in CESM2 versus CESM1: Monthly mean difference in the (a, c, e) thermodynamic and (b, d, f) dynamic contributions to ice volume tendency dV/dt, in cm/day, between CESM2 and CESM1 (i.e. CESM2 minus CESM1). Shown for (a, b) April, (c, d) June, and (e,f) August. In all panels, the solid black contour indicates sea ice extent in CESM2, and the dotted black contour indicates sea ice extent in CESM1.

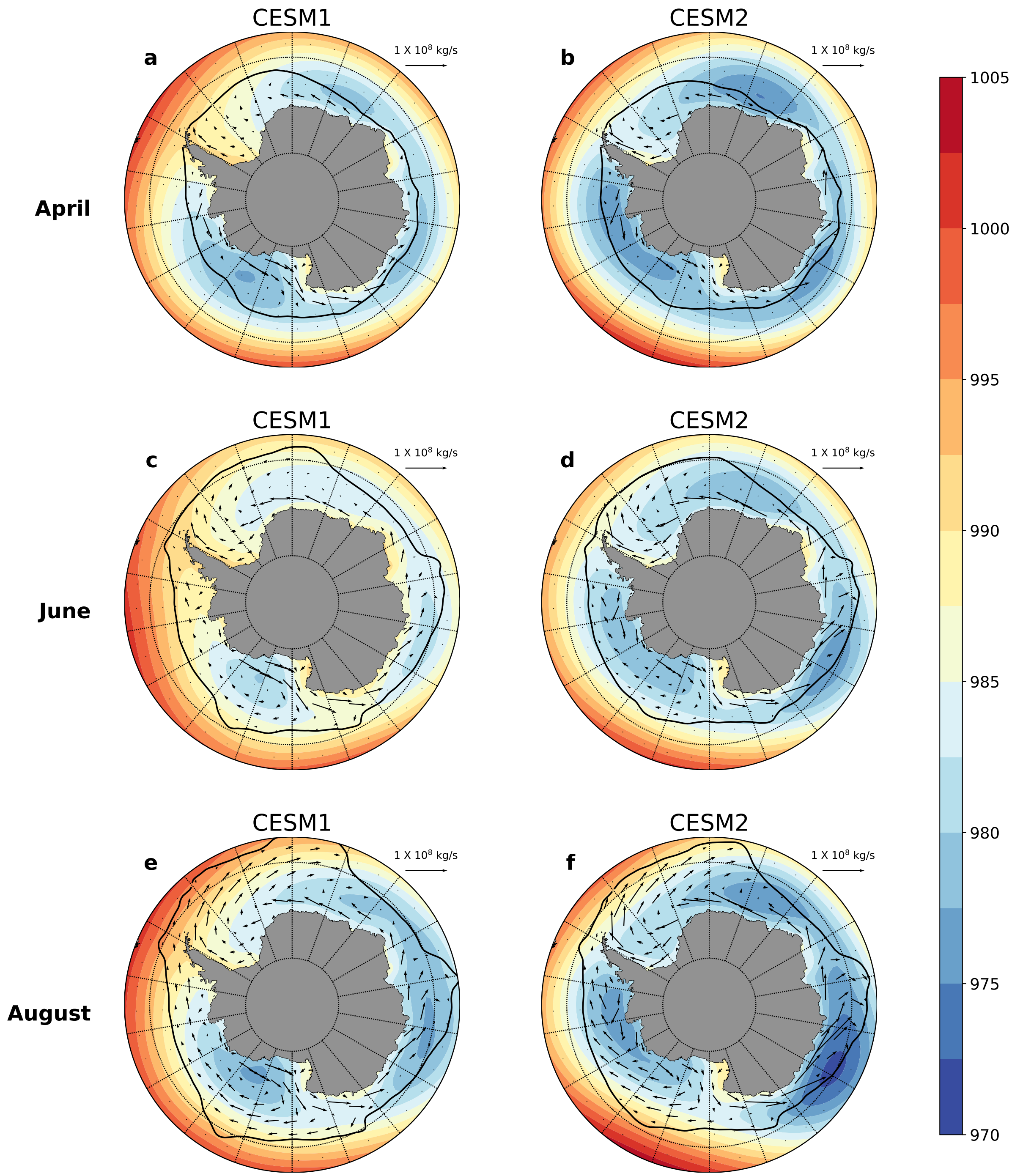

Figure 13. Antarctic Sea Ice Transport and Sea Level Pressure during the Growth Season: Monthly mean sea ice transport (vectors; scaled by 10^8 kg/s) and sea level pressure (colors; in hPa) in the (a, c, e) CESM1 and (b, d, f) CESM2, in (a, b) April, (c, d) June, and (e, f) August.

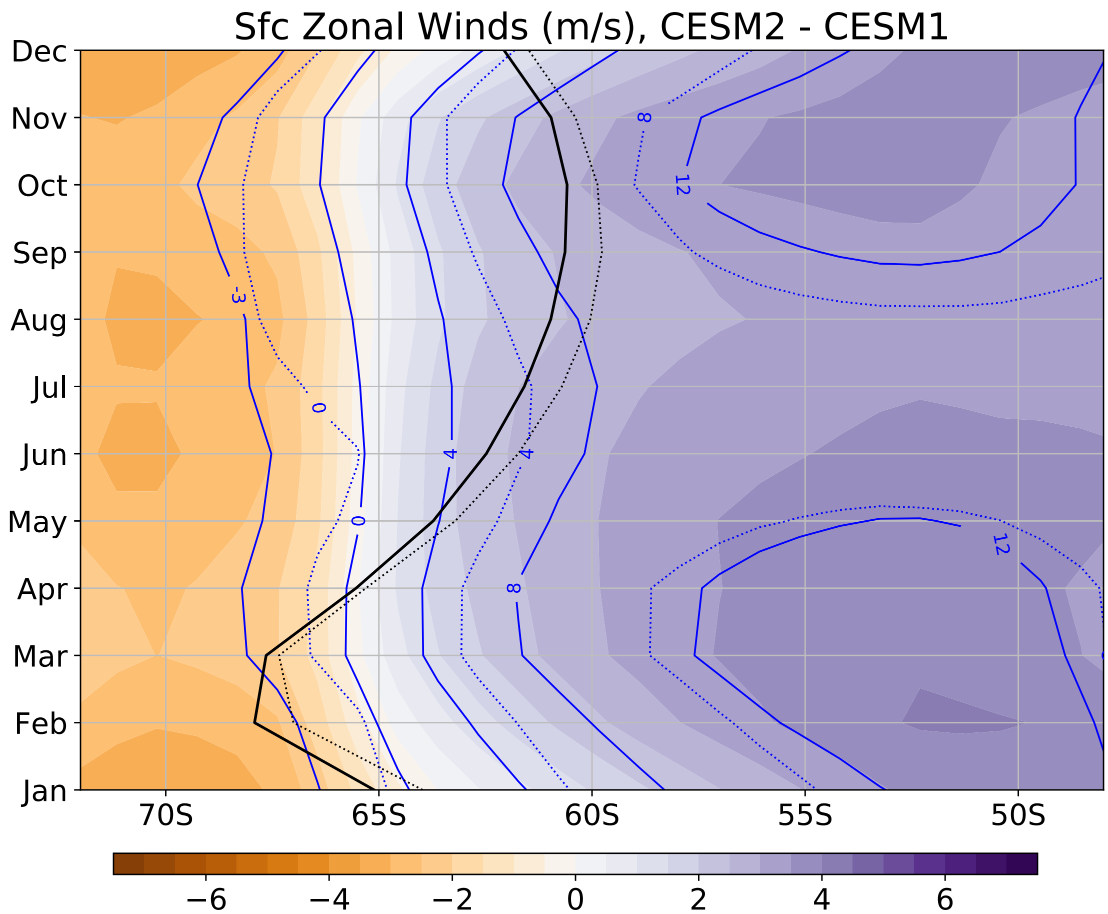

Figure 14. Zonal Winds at the Surface: Difference between the monthly zonal mean surface zonal winds in CESM2 and CESM1 (in m/sec; colors). Blue solid and dotted contours (at -3, 0, 4, 8, 12 m/s) show the monthly zonal mean surface zonal winds in CESM2 and CESM1, respectively. The monthly zonal mean ice extent (0.15 ice fraction isoline) for CESM2 (CESM1) is indicated by the solid (dotted) black contour.

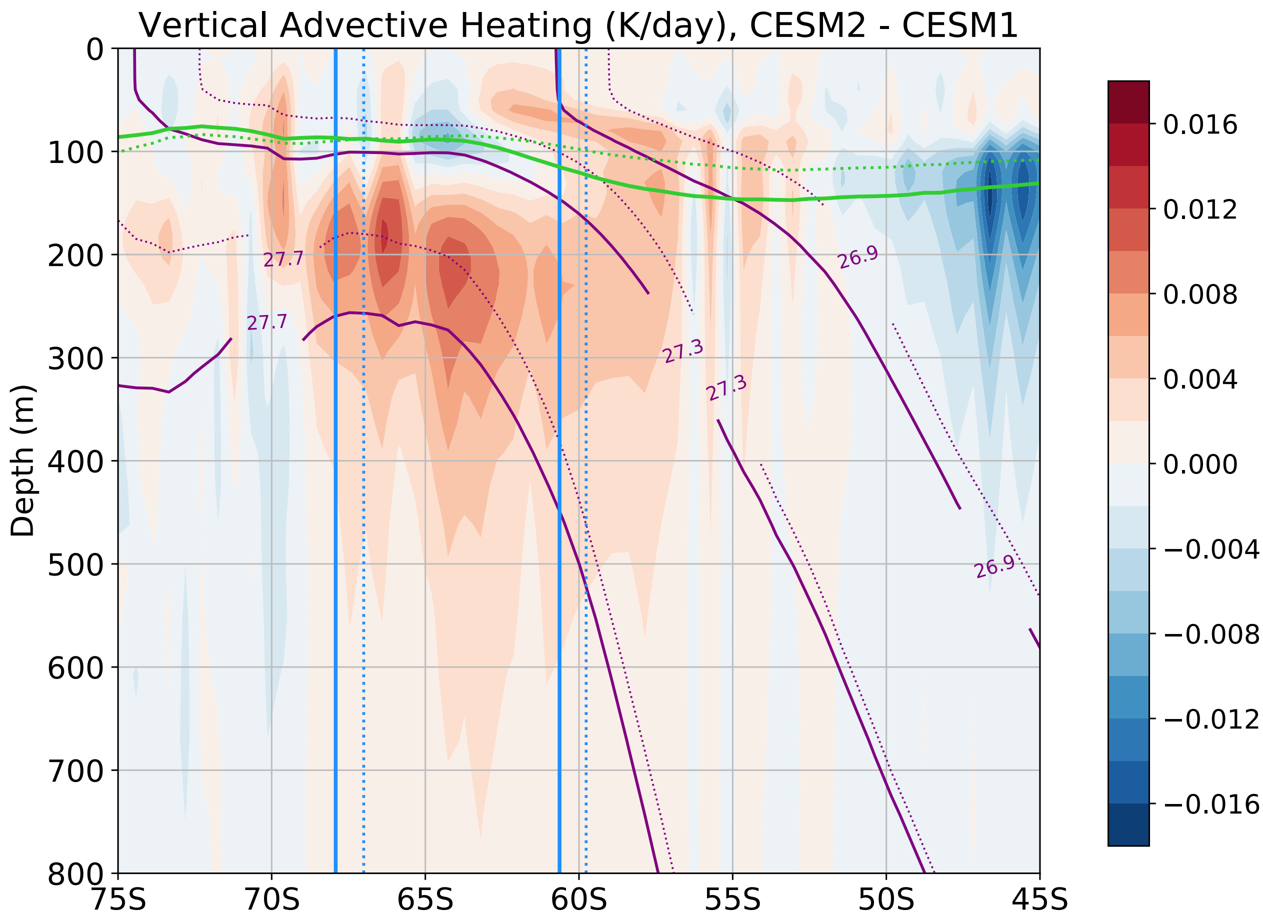

Figure 15. Heating by Upwelling during the Sea Ice Growth Season: Difference between ocean heating due to advection in CESM2 and CESM1 (in K/day; colors) over the growth season (March to August). Isopycnal surfaces (at $\sigma = 27.7, 27.3, 26.9$ kg/m^3) in CESM2 and CESM1 are shown by the purple solid and dotted contours, respectively. The blue solid (dotted) lines show the range of the ice extent in CESM2 (CESM1) from March to August, and the green solid (dotted) line indicates the zonal mean mixed layer depth in CESM2 (CESM1) over the growth season; the base of the mixed layer is reckoned as the interpolated depth to which surface-driven turbulence penetrates (see Danabasoglu et al., 2012).

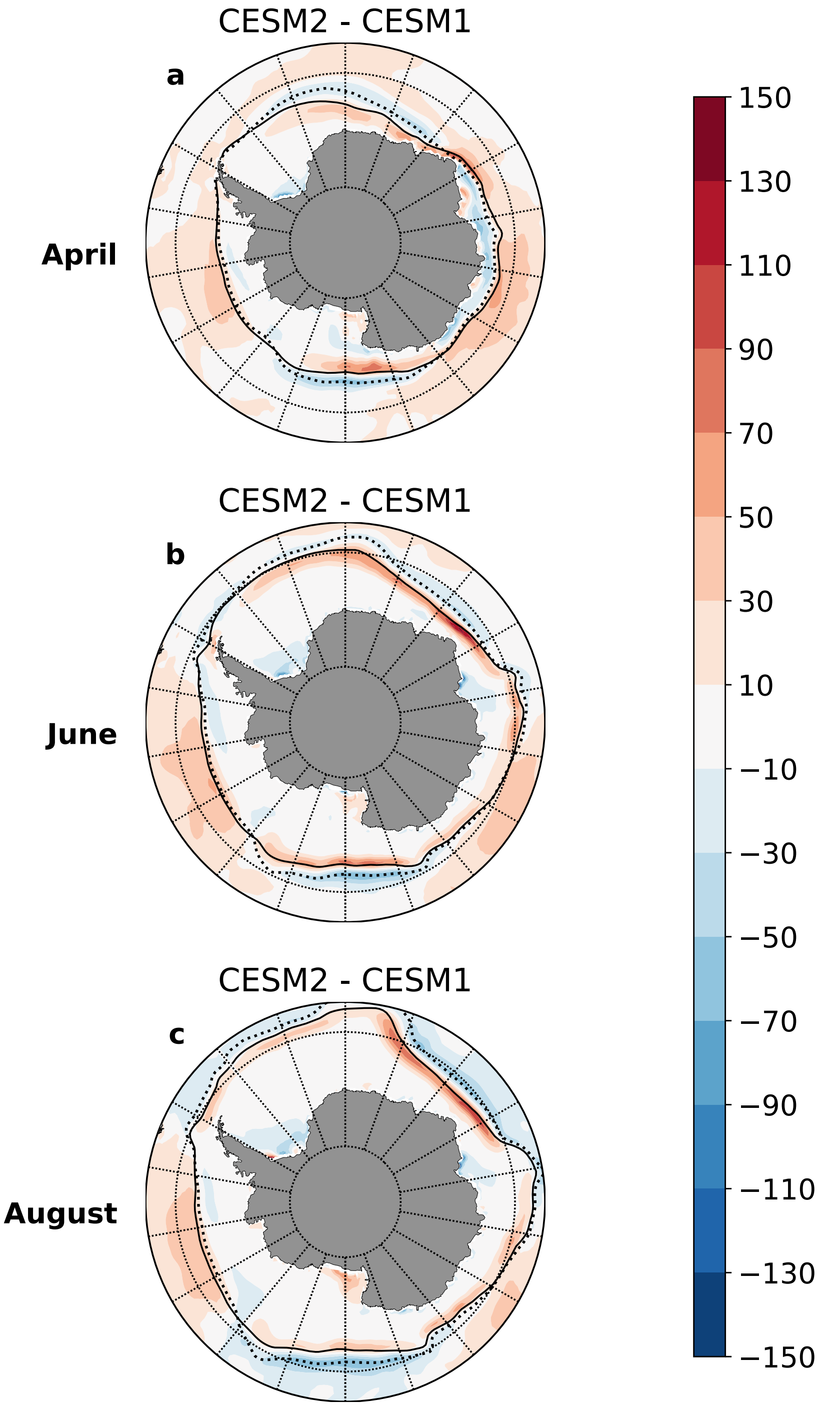

Figure 16. **Ocean Heat Flux Convergence during the Sea Ice Growth Season:** Difference between the monthly mean ocean heat flux convergence into the ocean mixed layer in CESM2 and CESM1 (in W/m^2; colors) in (a) April, (b) June, and (c) August. Solid and dashed contours in each panel show the sea ice extent in CESM2 and CESM1, respectively.

Figure 1.

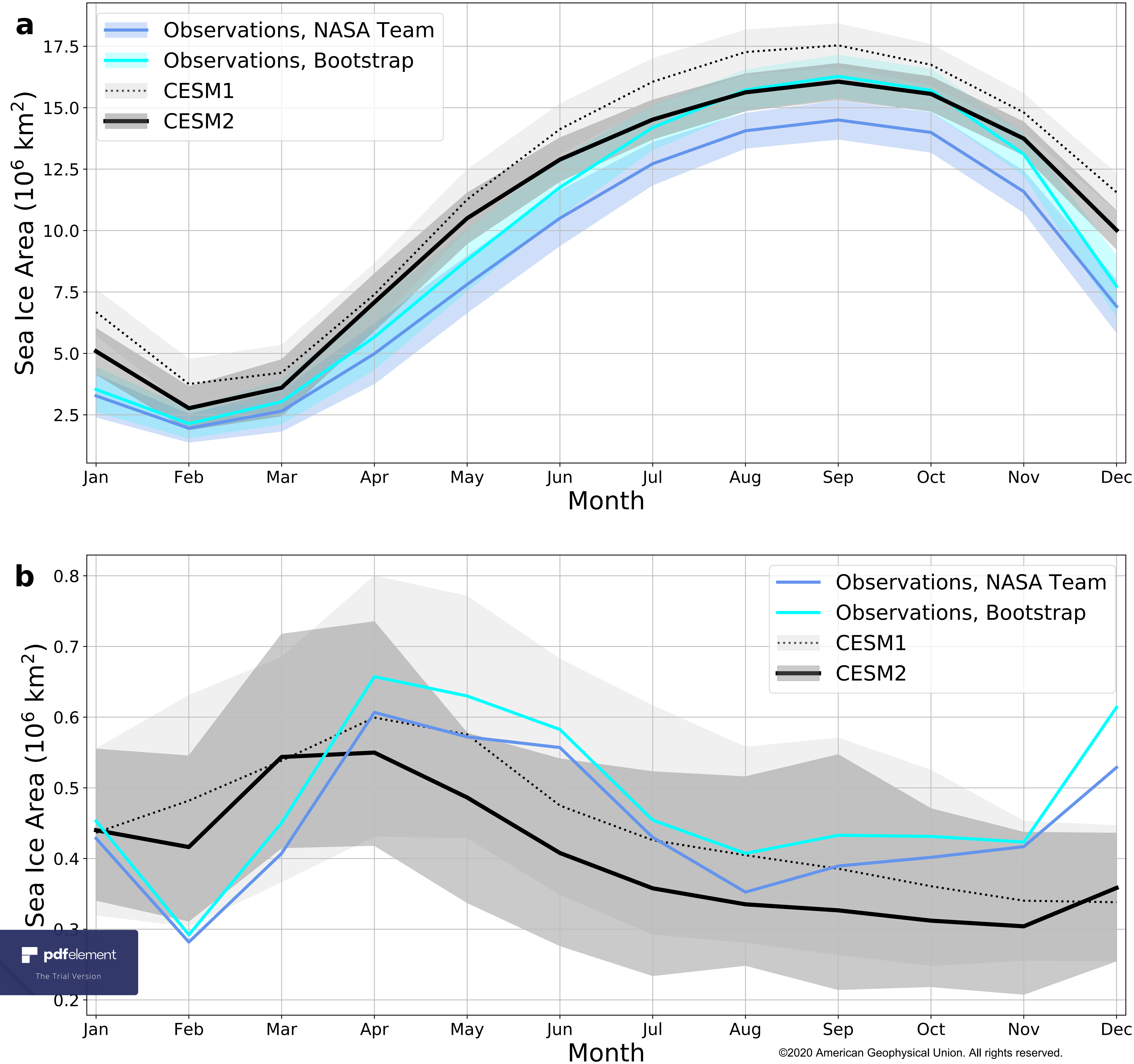

a
Observations, NASA Team
Observations, Bootstrap
CESM1
CESM2
Sea Ice Area (10^6 km^2)
Month
Jan
Feb
Mar
Apr
May
Jun
Jul
Aug
Sep
Oct
Nov
Dec
b
Observations, NASA Team
Observations, Bootstrap
CESM1
CESM2
Sea Ice Area (10^6 km^2)
Month

Figure 2.

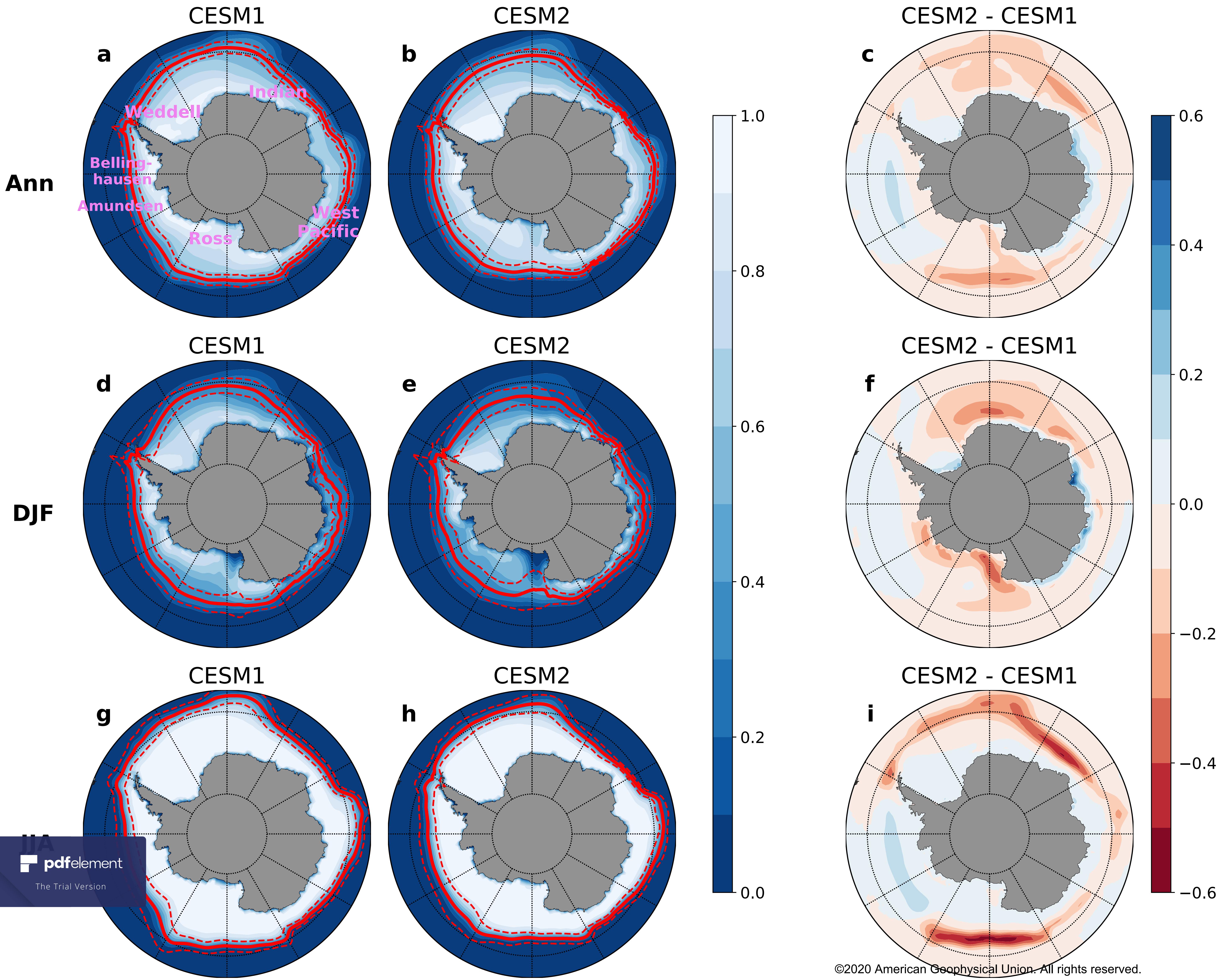

CESM1
CESM2
CESM2 - CESM1
a
b
c
Ann
Weddell
Indian
Belling-
hausen
Amundsen
Ross
West
Pacific
d
e
f
DJF
g
h
i
JJA
1.0
0.8
0.6
0.4
0.2
0.0
0.6
0.4
0.2
0.0
−0.2
−0.4
−0.6

Figure 3.

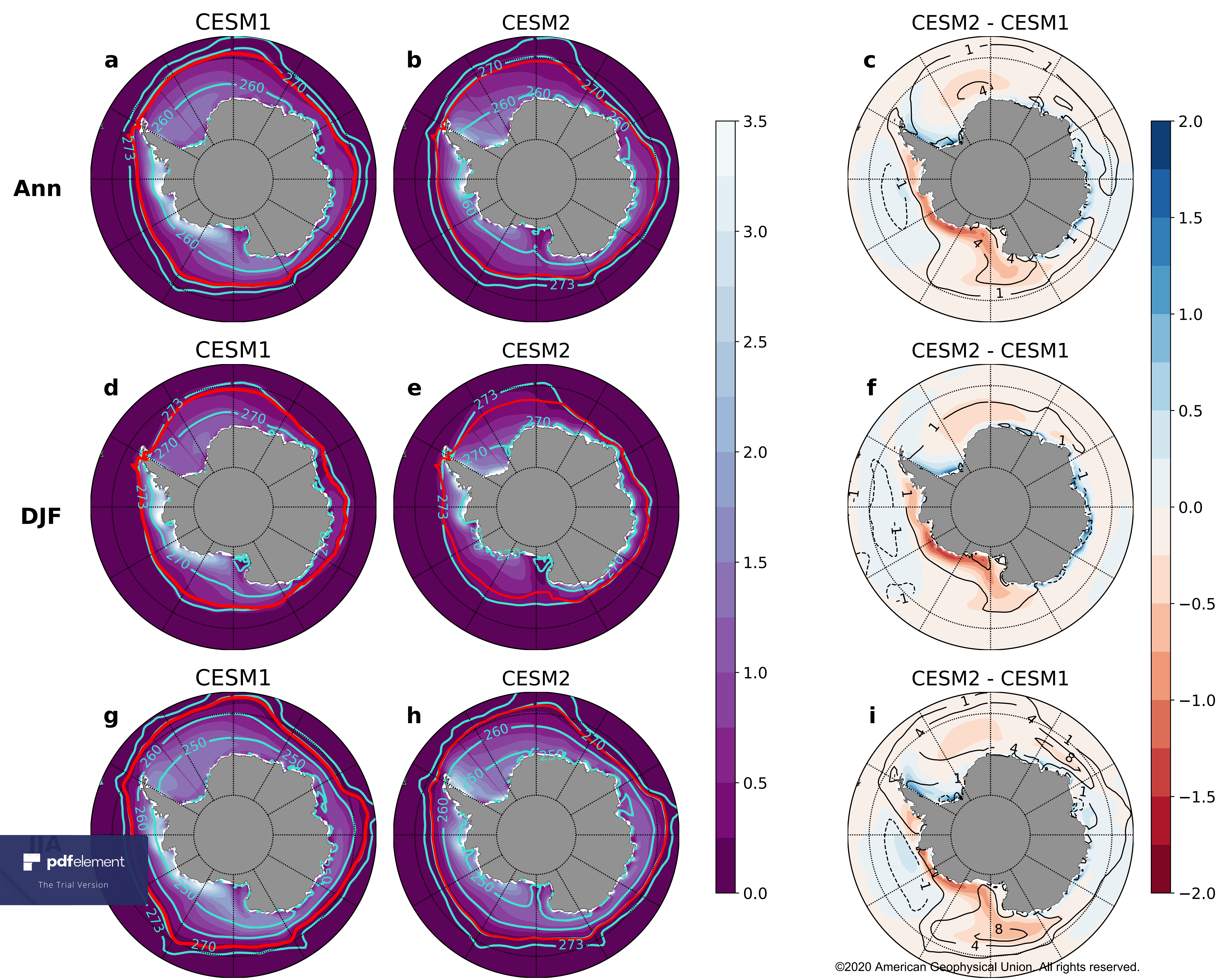

CESM1
CESM2
CESM2 - CESM1
a
b
c
Ann
d
e
f
DJF
g
h
i
JJA

Figure 4.

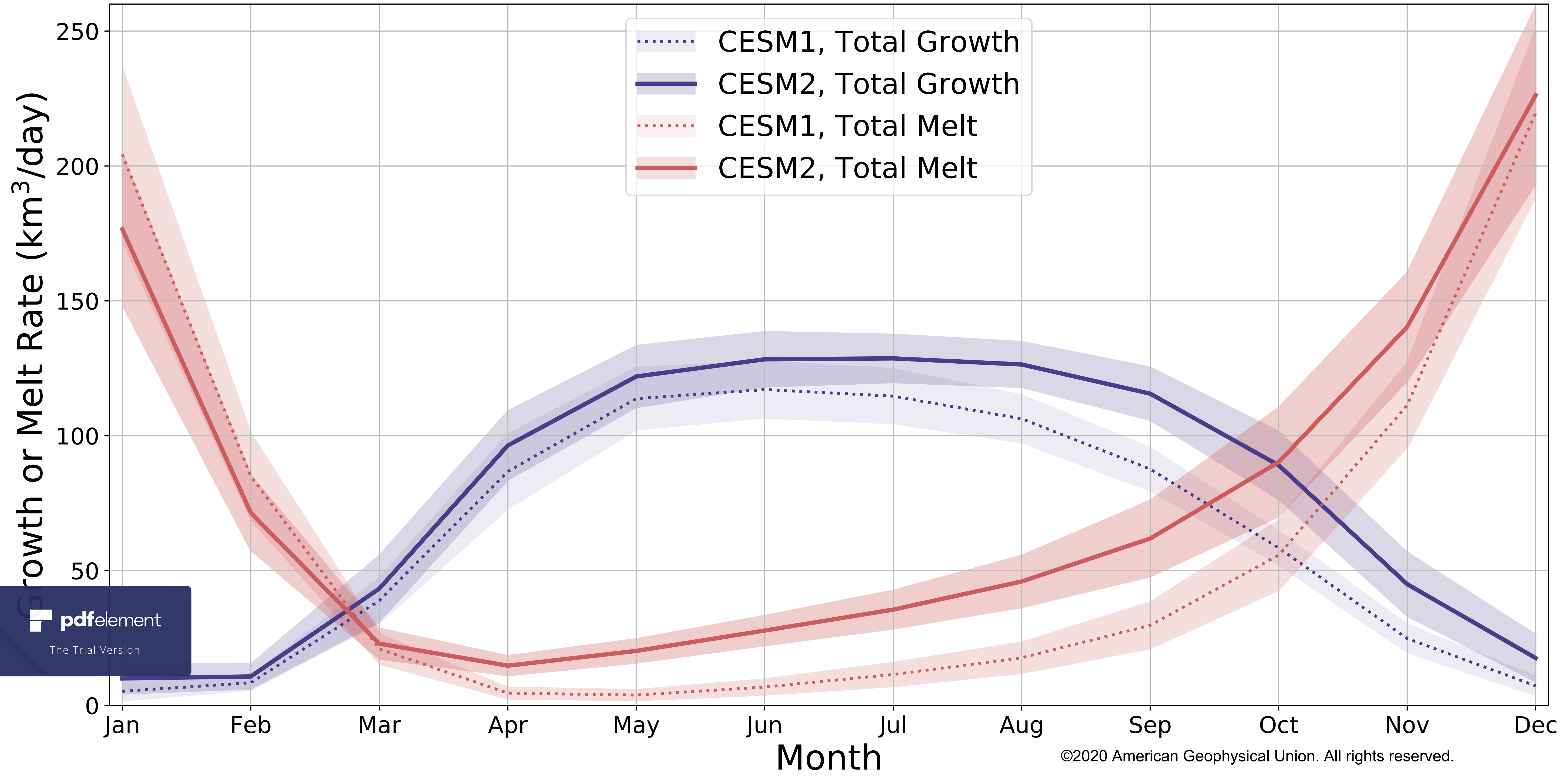
CESM1, Total Growth
CESM2, Total Growth
CESM1, Total Melt
CESM2, Total Melt
Growth or Melt Rate (km^3/day)
250
200
150
100
50
0
Jan
Feb
Mar
Apr
May
Jun
Jul
Aug
Sep
Oct
Nov
Dec
Month
pdfelement
The Trial Version

Figure 5.

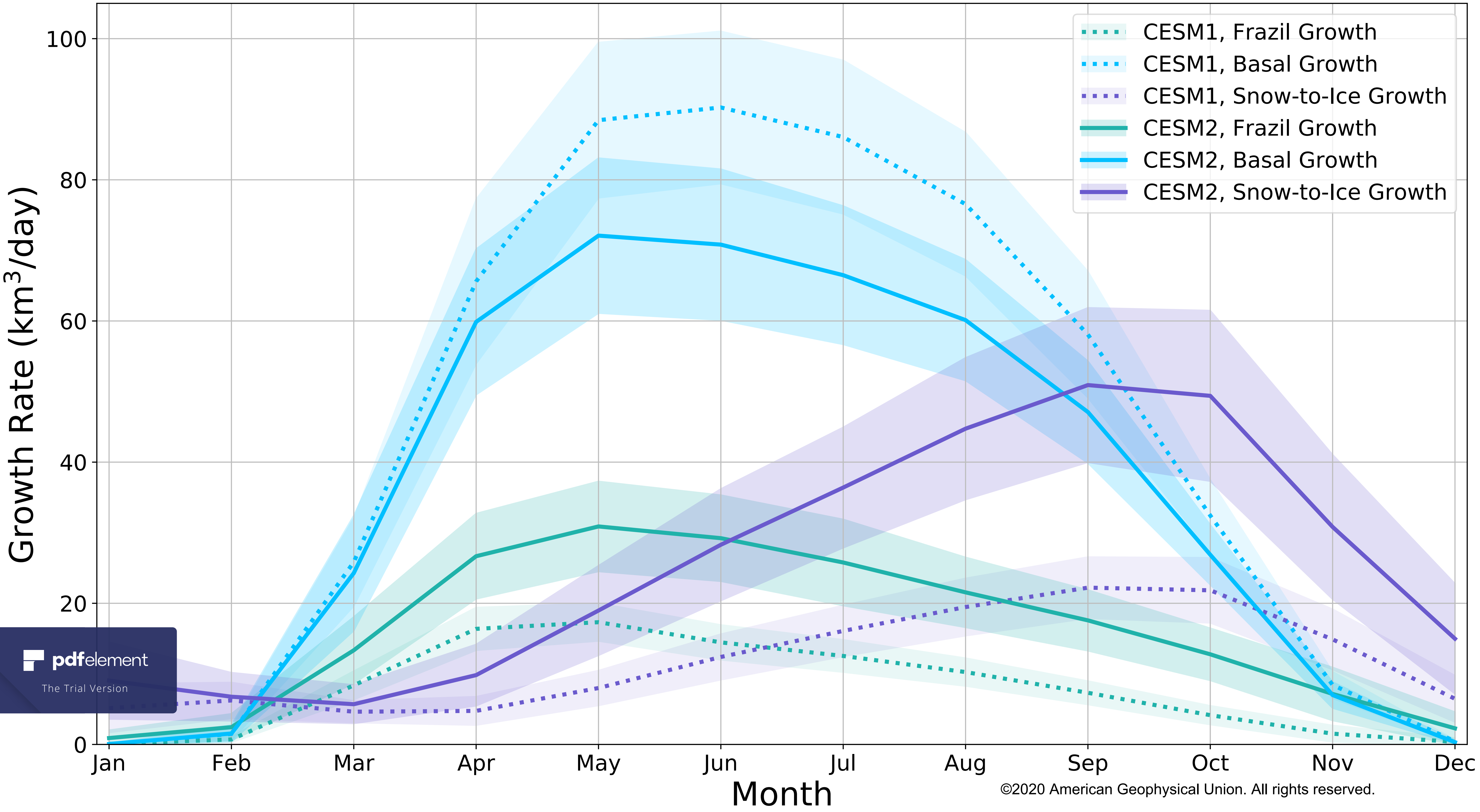
CESM1, Frazil Growth
CESM1, Basal Growth
CESM1, Snow-to-Ice Growth
CESM2, Frazil Growth
CESM2, Basal Growth
CESM2, Snow-to-Ice Growth
Growth Rate (km^3/day)
0
20
40
60
80
100
Jan
Feb
Mar
Apr
May
Jun
Jul
Aug
Sep
Oct
Nov
Dec
Month

Figure 6.

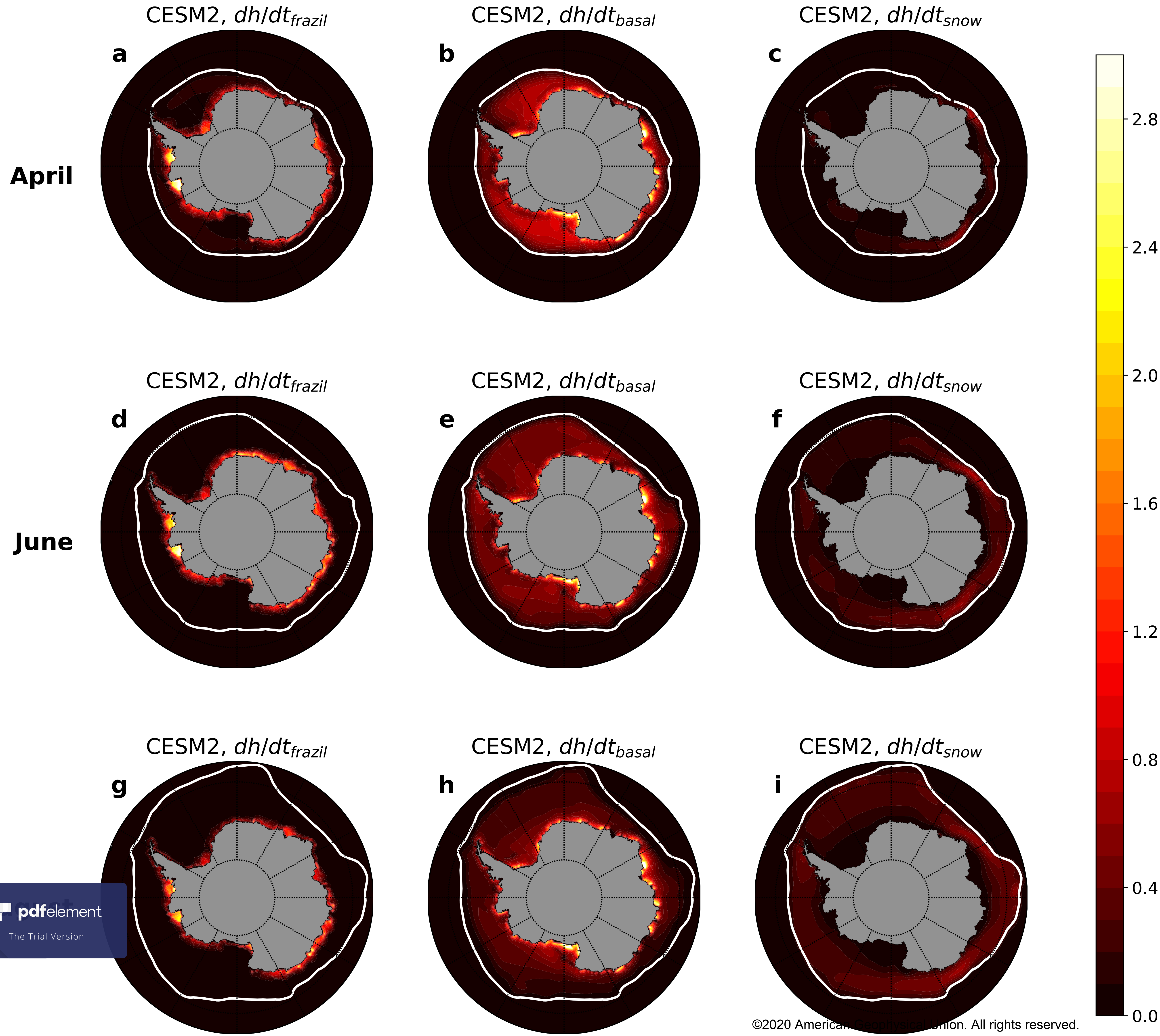

CESM2, dh/dt_{frazil}
CESM2, dh/dt_{basal}
CESM2, dh/dt_{snow}
a
b
c
April
d
e
f
June
g
h
i
August
0.0
0.4
0.8
1.2
1.6
2.0
2.4
2.8

Figure 7.

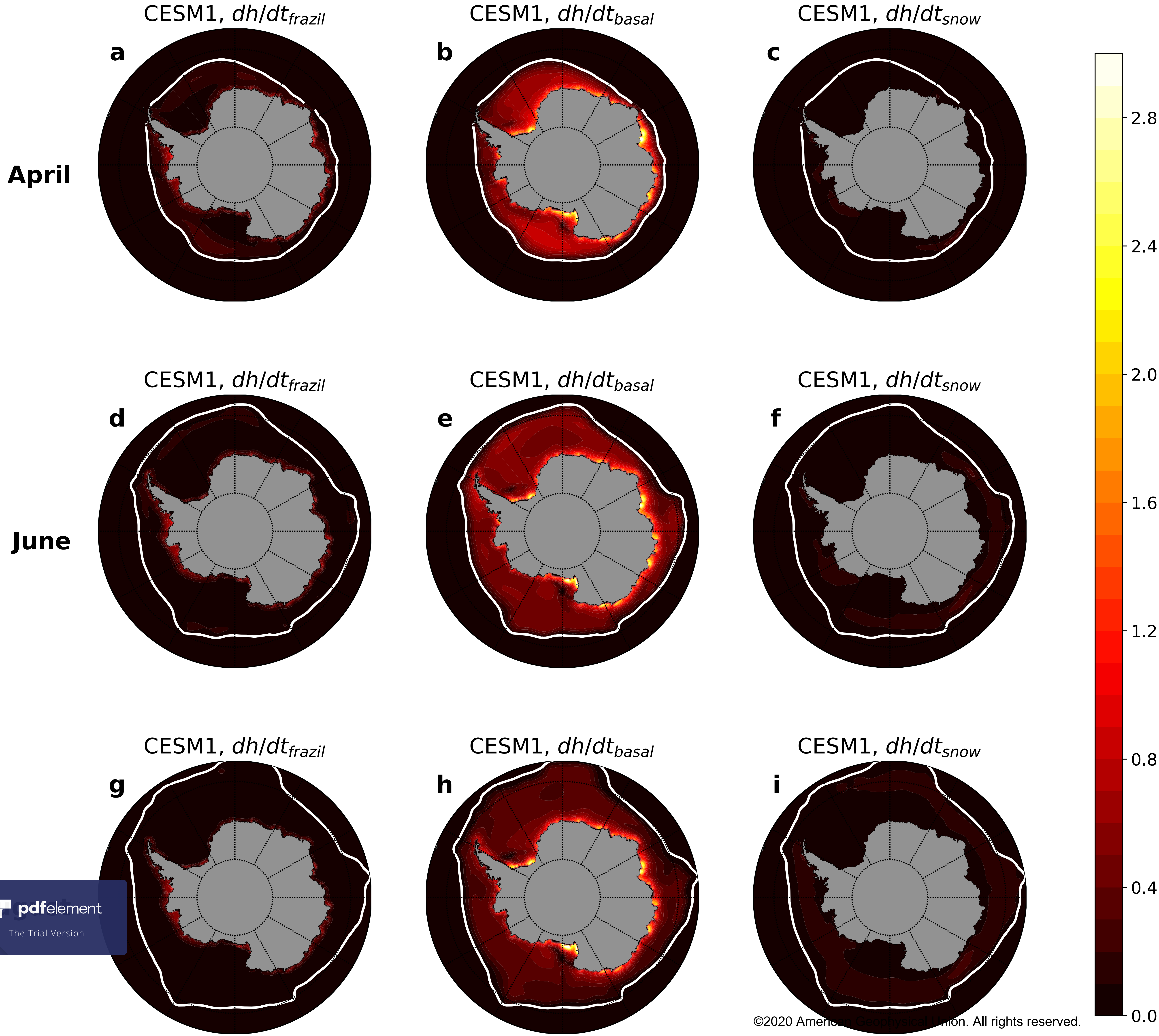
CESM1, dh/dt_{frazil}
CESM1, dh/dt_{basal}
CESM1, dh/dt_{snow}
a
b
c
April
CESM1, dh/dt_{frazil}
CESM1, dh/dt_{basal}
CESM1, dh/dt_{snow}
d
e
f
June
CESM1, dh/dt_{frazil}
CESM1, dh/dt_{basal}
CESM1, dh/dt_{snow}
g
h
i
2.8
2.4
2.0
1.6
1.2
0.8
0.4
0.0

Figure 8.

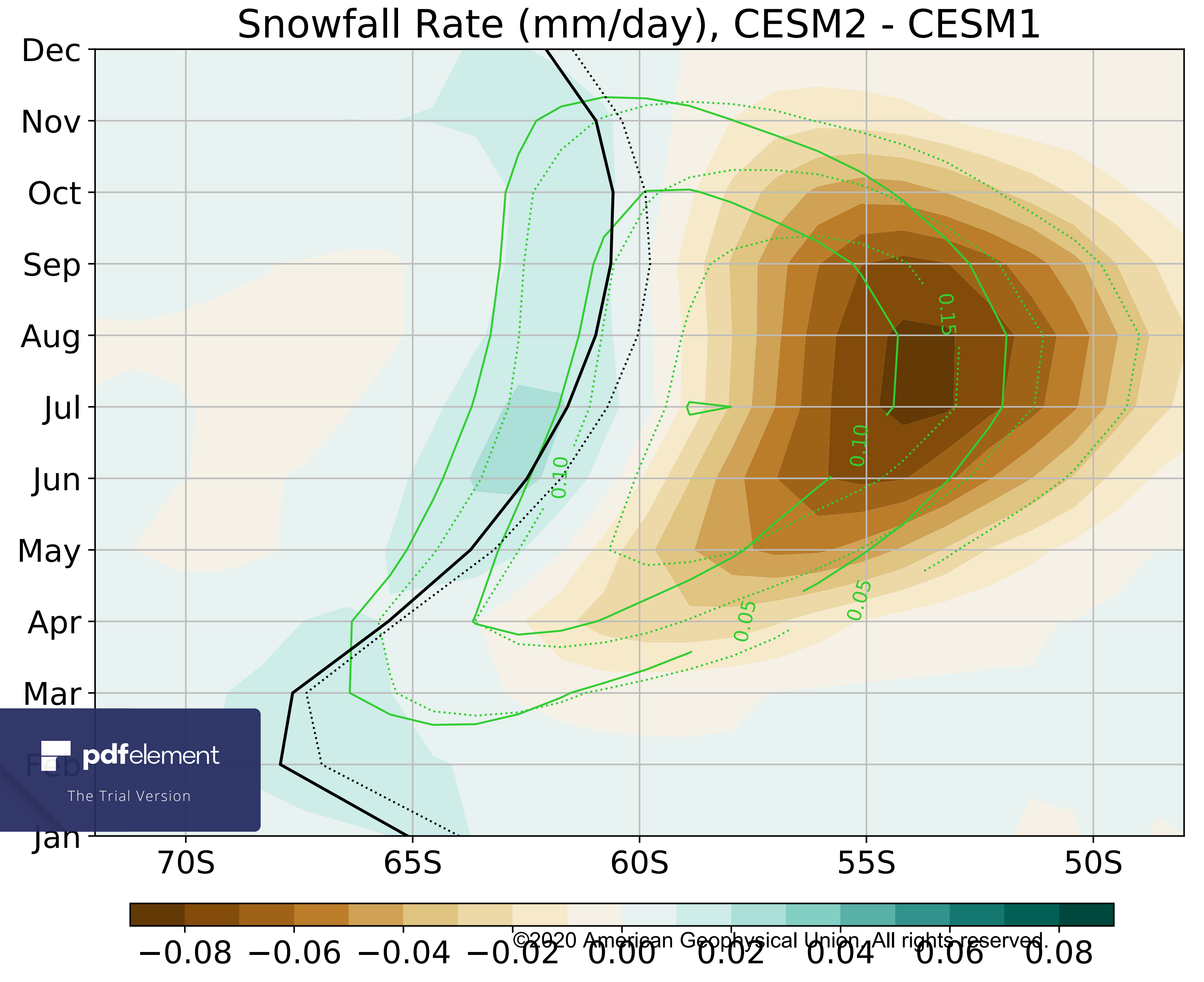

Snowfall Rate (mm/day), CESM2 - CESM1
Dec
Nov
Oct
Sep
Aug
Jul
Jun
May
Apr
Mar
Feb
Jan
70S
65S
60S
55S
50S
0.15
0.10
0.10
0.05
0.05
−0.08
−0.06
−0.04
−0.02
0.00
0.02
0.04
0.06
0.08
pdfelement
The Trial Version

Figure 9.

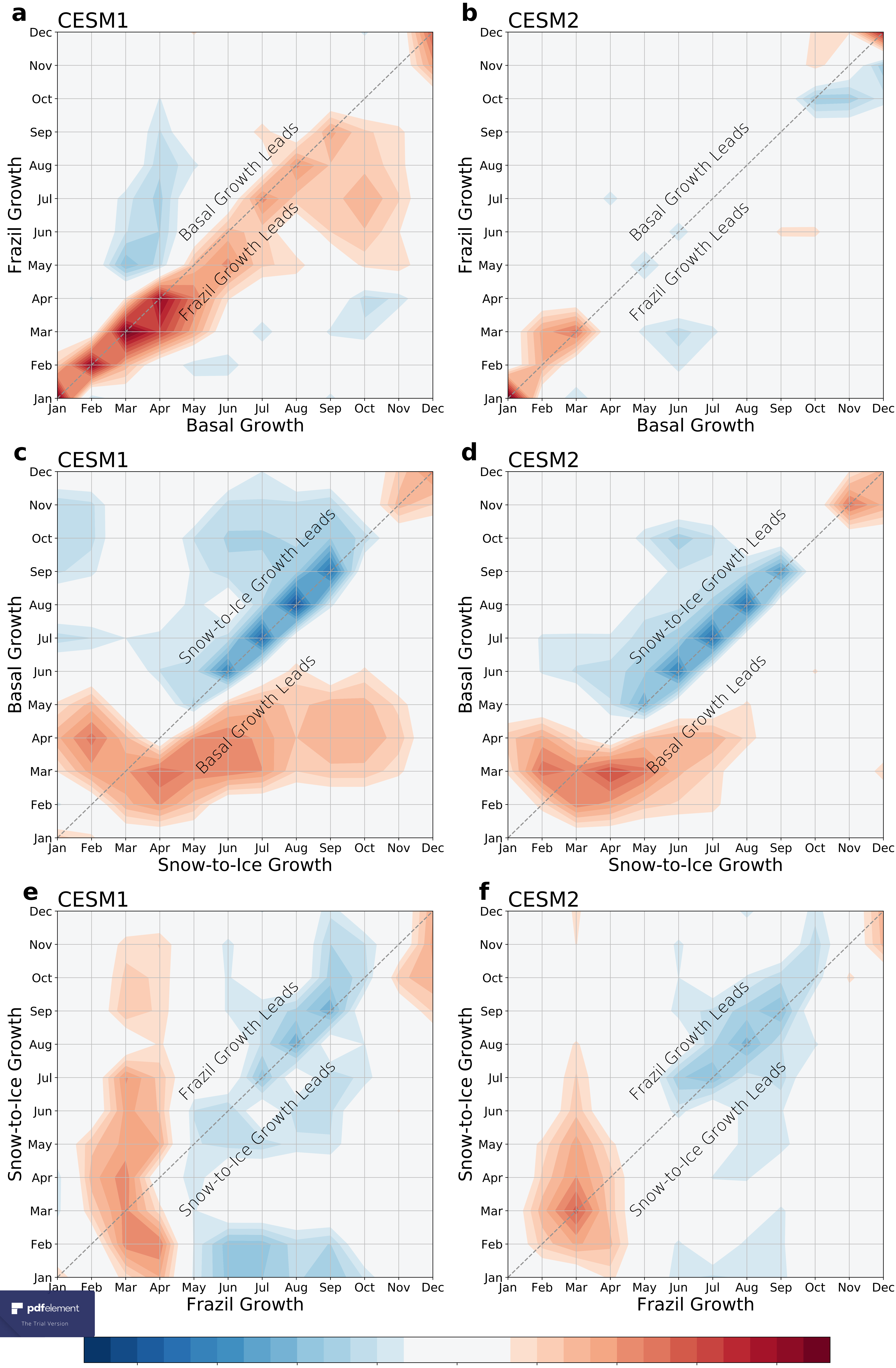

a CESM1
b CESM2
c CESM1
d CESM2
e CESM1
f CESM2
Frazil Growth
Basal Growth
Snow-to-Ice Growth
Basal Growth Leads
Frazil Growth Leads
Snow-to-Ice Growth Leads
Jan Feb Mar Apr May Jun Jul Aug Sep Oct Nov Dec
−0.60 −0.45 −0.30 −0.15 0.00 0.15 0.30 0.45 0.60

Figure 10.

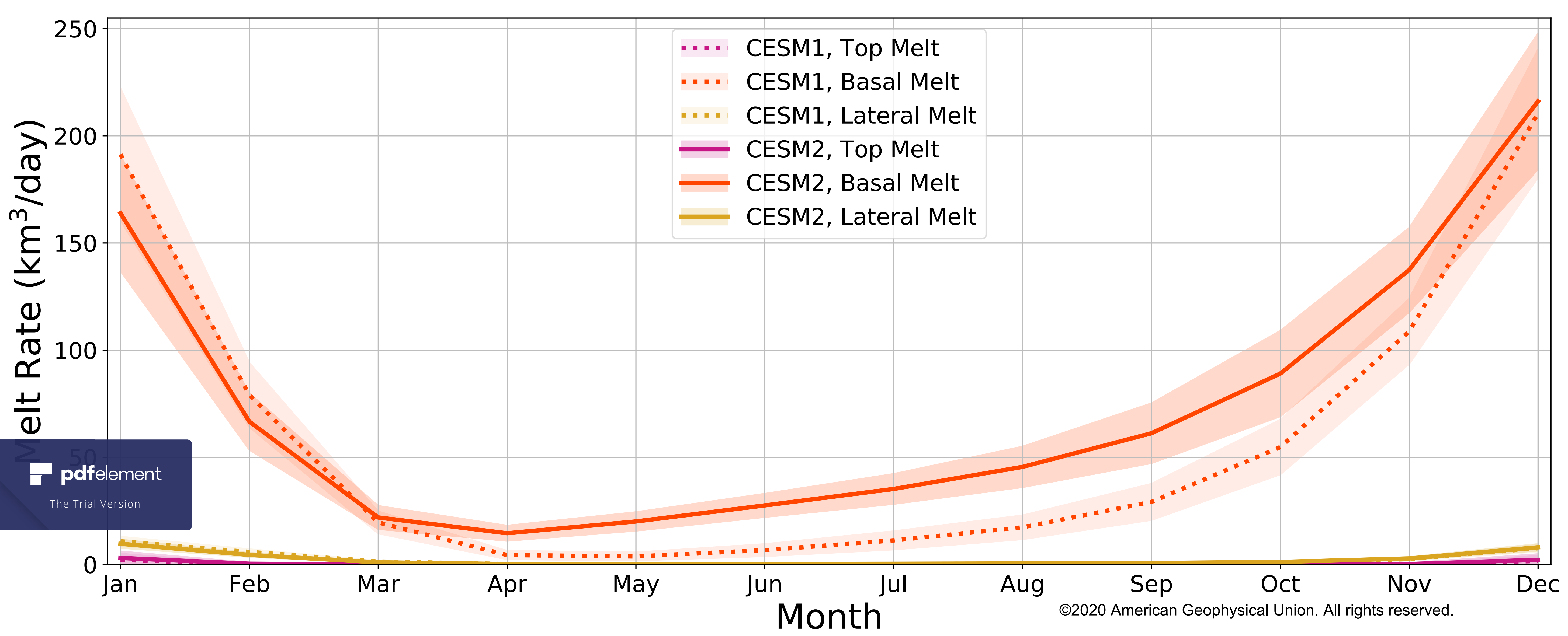
Melt Rate (km^3/day)
250
200
150
100
50
0
CESM1, Top Melt
CESM1, Basal Melt
CESM1, Lateral Melt
CESM2, Top Melt
CESM2, Basal Melt
CESM2, Lateral Melt
Jan
Feb
Mar
Apr
May
Jun
Jul
Aug
Sep
Oct
Nov
Dec
Month
pdfelement
The Trial Version

Figure 11.

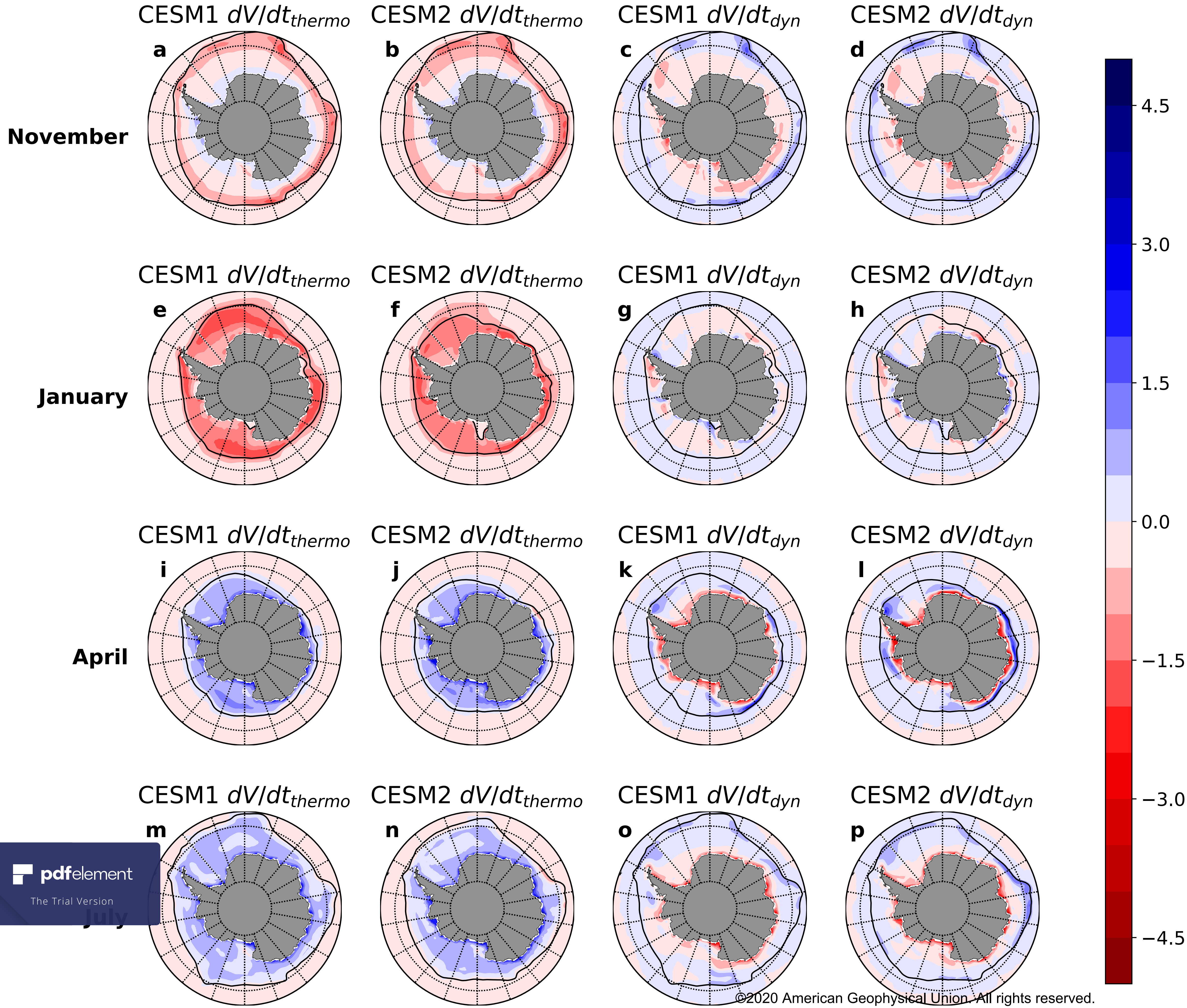

CESM1 dV/dt_{thermo}
CESM2 dV/dt_{thermo}
CESM1 dV/dt_{dyn}
CESM2 dV/dt_{dyn}
a
b
c
d
November
e
f
g
h
January
i
j
k
l
April
m
n
o
p
July
4.5
3.0
1.5
0.0
−1.5
−3.0
−4.5

Figure 12.

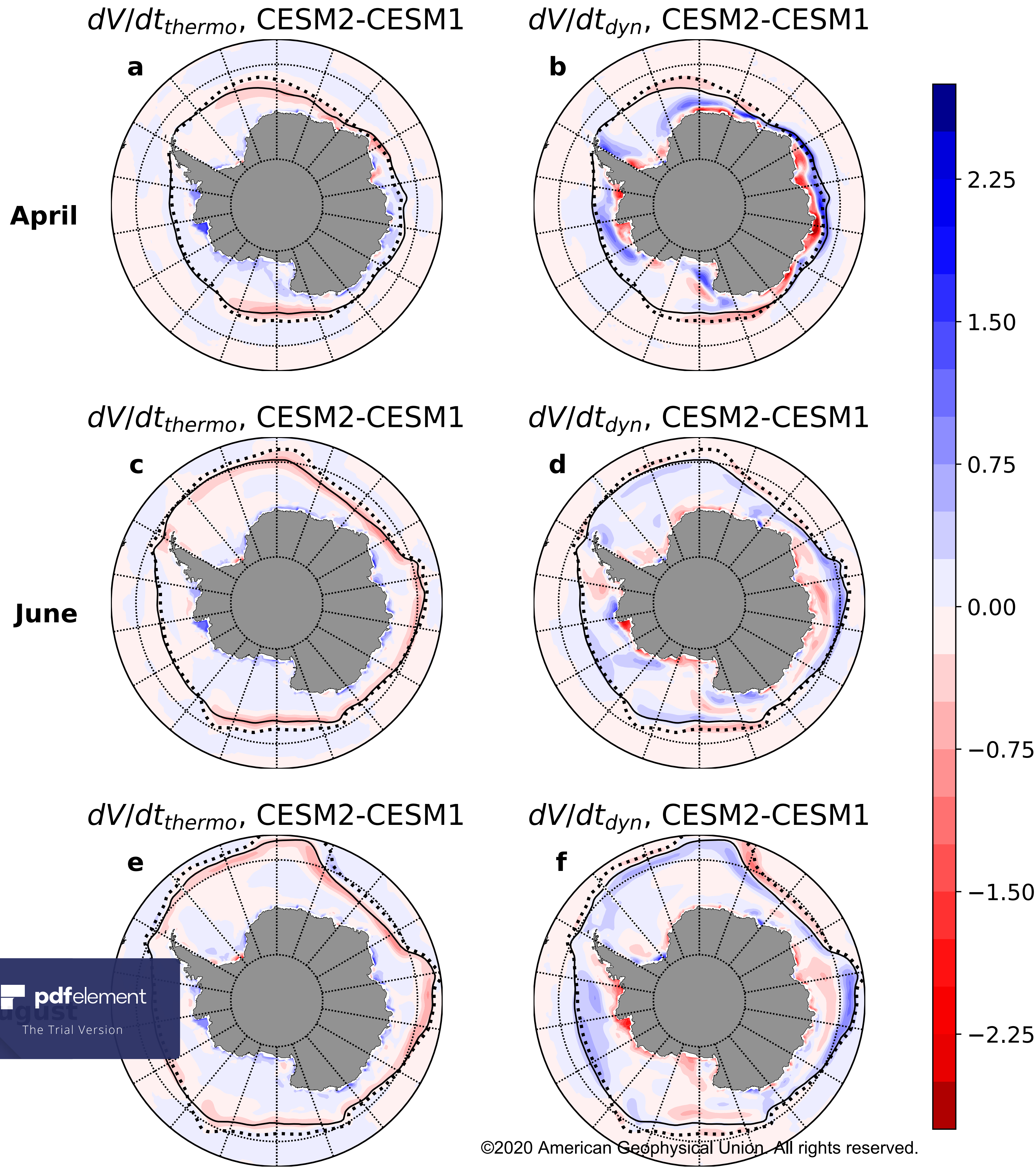

dV/dt_thermo, CESM2-CESM1
dV/dt_dyn, CESM2-CESM1
a
b
April
dV/dt_thermo, CESM2-CESM1
dV/dt_dyn, CESM2-CESM1
c
d
June
dV/dt_thermo, CESM2-CESM1
dV/dt_dyn, CESM2-CESM1
e
f
August
2.25
1.50
0.75
0.00
−0.75
−1.50
−2.25

Figure 13.

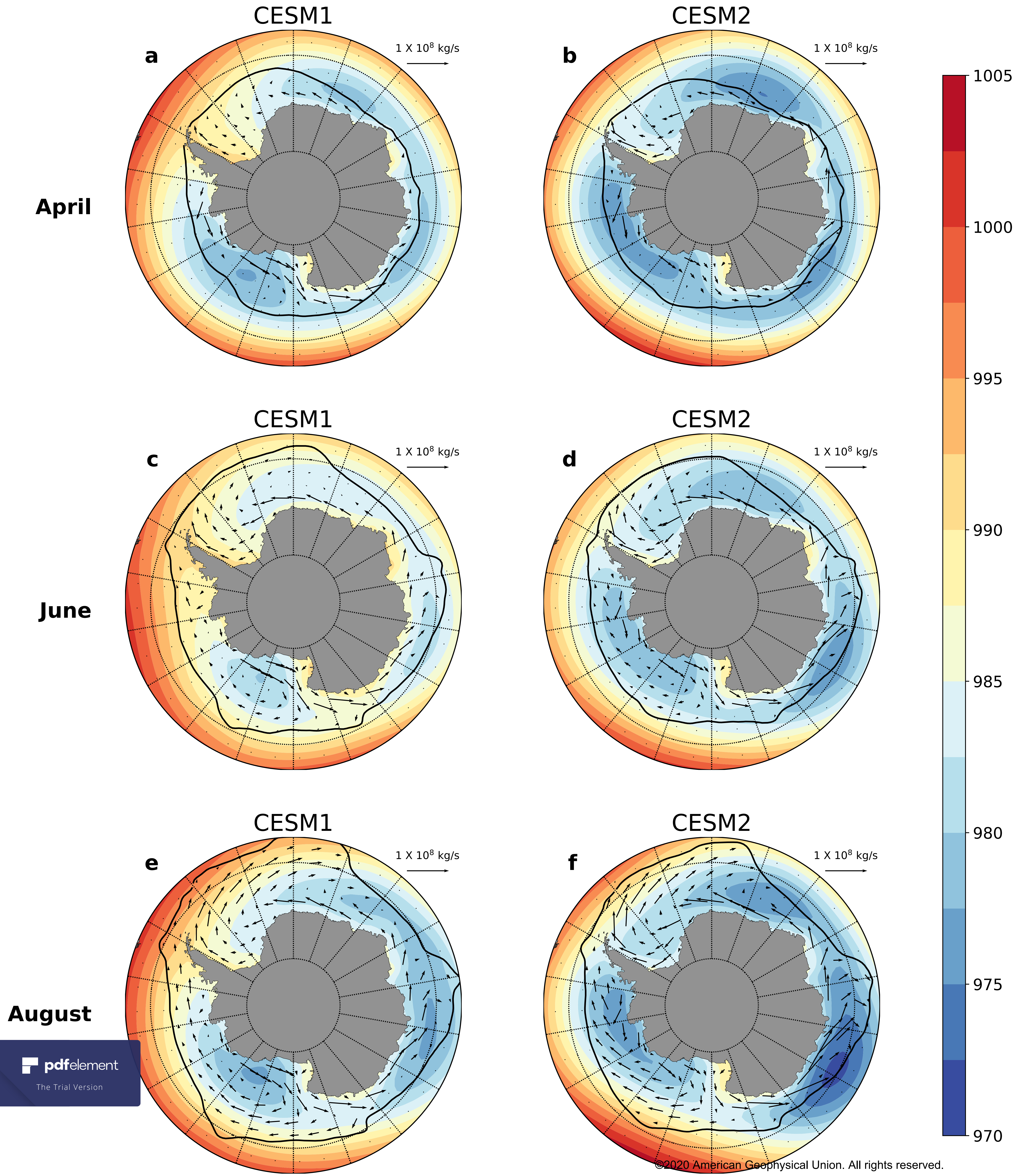
CESM1
CESM2
a
b
c
d
e
f
1 X 10^8 kg/s
April
June
August
1005
1000
995
990
985
980
975
970

Figure 14.

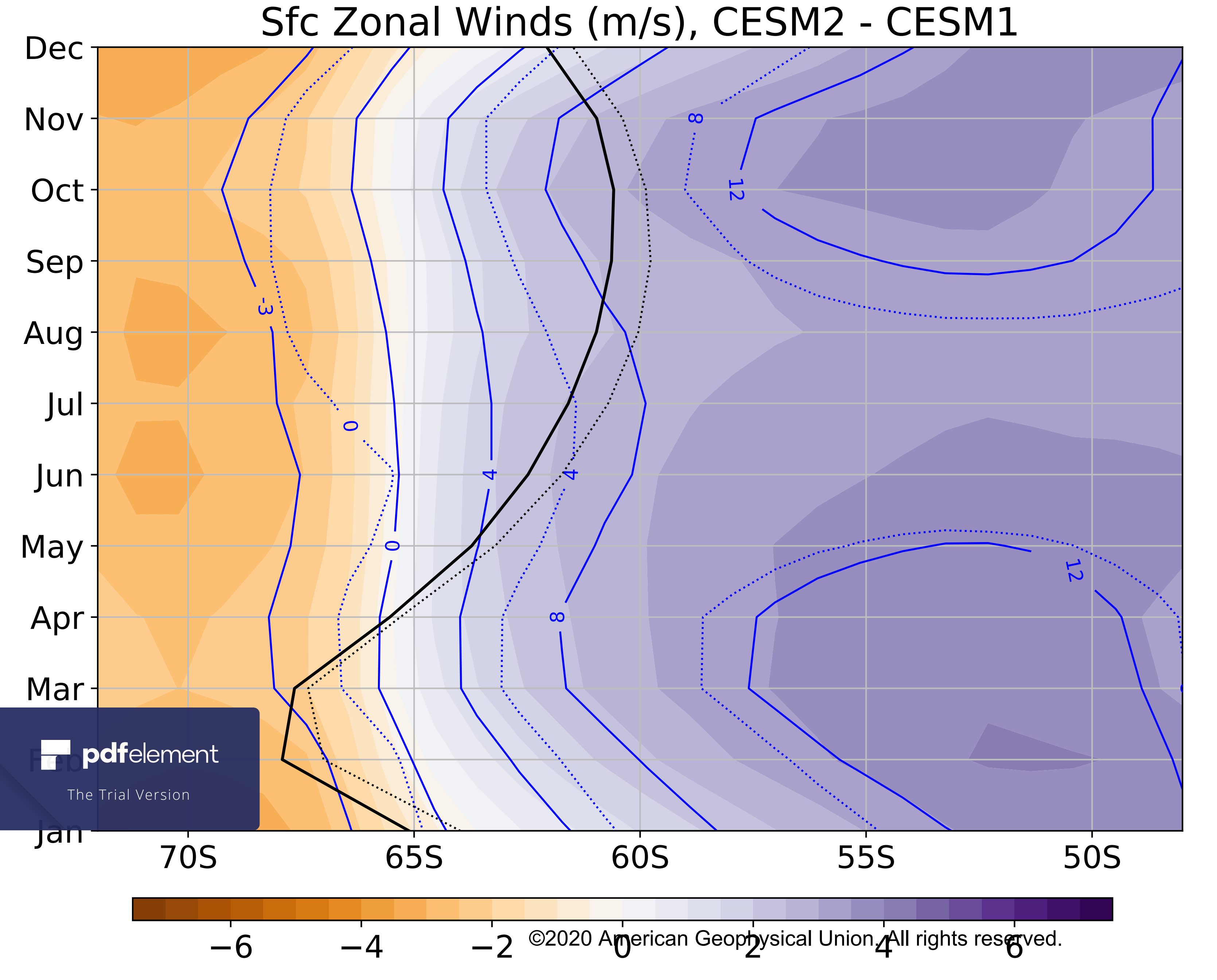
Sfc Zonal Winds (m/s), CESM2 - CESM1
Dec
Nov
Oct
Sep
Aug
Jul
Jun
May
Apr
Mar
Feb
Jan
70S
65S
60S
55S
50S
-3
0
4
8
12
−6
−4
−2
0
2
4
6

Figure 15.

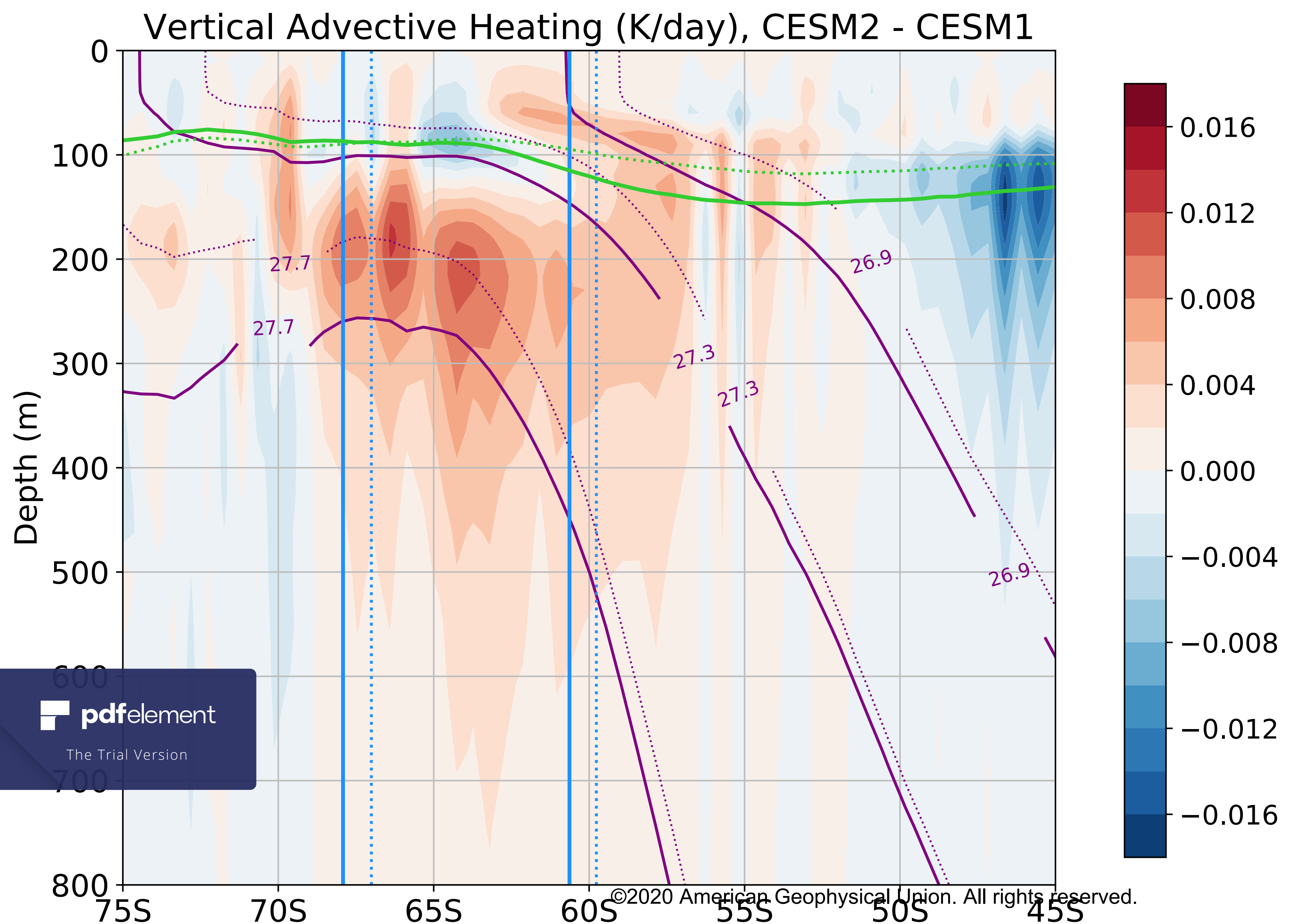

Vertical Advective Heating (K/day), CESM2 - CESM1
Depth (m)
0
100
200
300
400
500
600
700
800
75S
70S
65S
60S
55S
50S
45S
27.7
27.7
27.3
27.3
26.9
26.9
0.016
0.012
0.008
0.004
0.000
−0.004
−0.008
−0.012
−0.016

Figure 16.

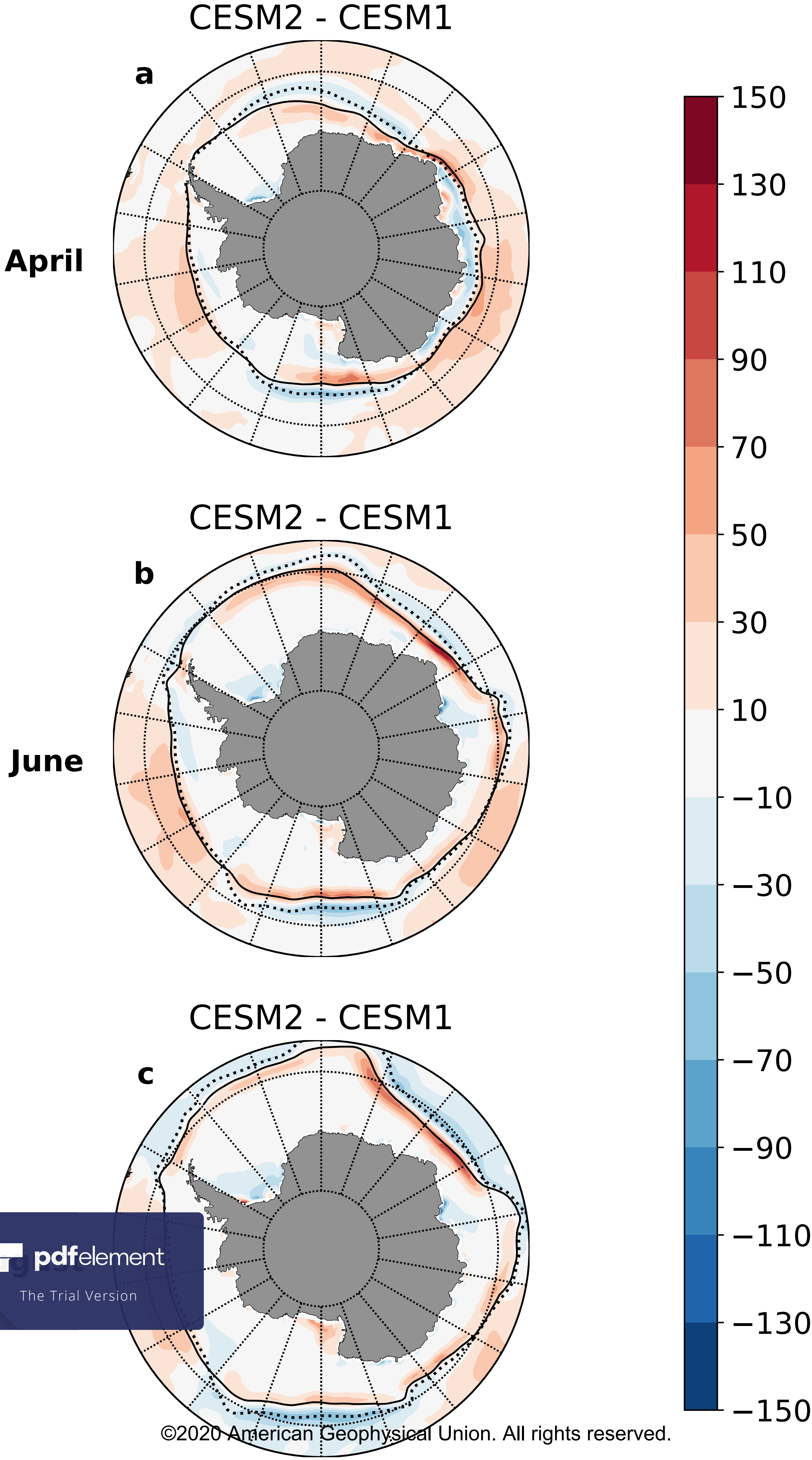
CESM2 - CESM1
a
April
CESM2 - CESM1
b
June
CESM2 - CESM1
c
150
130
110
90
70
50
30
10
−10
−30
−50
−70
−90
−110
−130
−150